UNIVERSITÀ DEGLI STUDI DI PADOVA

Dipartimento di Biologia

SCUOLA DI DOTTORATO DI RICERCA IN: Bioscienze e Biotecnologie

INDIRIZZO: Biologia cellulare

CICLO XXVII

Identification and characterization of atlastin interacting partners involved in maintaining and determining the morphology of endoplasmic reticulum in *Drosophila melanogaster*

Direttore della Scuola: Ch.mo Prof. Giuseppe Zanotti

Coordinatore d'indirizzo: Ch.mo Prof. Paolo Bernardi

Supervisore: Ch.mo Prof. Cesare Montecucco

Co-supervisore: Dott. Andrea Daga

Dottorando: Giulia Misticoni

INDEX

ABSTRACT ..... **VII**

RIASSUNTO ..... **IX**

1 INTRODUCTION **1**

1.1 Mechanisms of membrane fusion and fission 1

1.1.1 Proteins driving fusion 3

1.1.2 Intracellular membrane fusion 4

1.1.3 Mitochondrial membrane dynamics 4

1.1.4 Proteins driving fission 5

1.2 Endoplasmic reticulum 8

1.2.1 ER structure and organization 8

1.2.2 The ER is a single compartment 9

1.2.3 Propagation of the ER during mitosis 9

1.2.4 ER dynamics 10

1.3 Atlastin 14

1.3.1 SPG3A gene 14

1.3.2 Atlastin subfamily 15

1.3.3 Atlastin structure 15

1.3.4 Human atlastins 16

1.3.5 *Drosophila* atlastin 17

1.4 Reticulon and DP1 20

1.4.1 Reticulon and DP1 family 20

1.4.2 Reticulon and DP1 structure 21

1.4.3 Reticulon and DP1: protein localization and function 22

1.4.4 Reticulon and DP1 in *Arabidopsis thaliana* 24

1.4.5 *Drosophila* reticulon 25

1.5 Atlastin functional partners 26

1.6 *Drosophila* as a model organism 26

2 METHODS 29

2.1 Molecular biology techniques: generation of constructs 29

2.1.1 Cloning of Rtnl1 cDNA in pcDNA3.1/Zeo(+) plasmid 29

2.1.2 Cloning of Rtnl1 cDNA in pUAST plasmid 32

2.1.3 Cloning of Rtnl1 cDNA in pGEX-GST-SUMO1 plasmid 33

2.1.4 Amplification of DP1 cDNA 35

2.1.5 Cloning of DP1 cDNA in pcDNA3.1/Zeo(+) plasmid 36

2.1.6 Cloning of DP1 cDNA in pUAST plasmid 38

2.1.7 Cloning of Atlastin cDNA in pcDNA3.1/Zeo(+) plasmid 40

2.2 Quantitative Real-Time PCR 40

2.3 Biochemical techniques 42

2.3.1 Rtnl1 protein purification 42

2.4 Cellular biology 42

2.4.1 Cell culture 42

2.4.2 Propagation and subculturing 43

2.4.3 Plasmid DNA Transfection 43

2.4.4 Immunocytochemistry (ICC) 44

2.5 Microscopy 46

2.5.1 Immunohistochemistry 46

2.5.2 Fluorescence loss in photobleaching (FLIP) 46

2.5.3 Image analysis 46

2.5.4 Electron microscopy 46

2.6 *Drosophila* transformation 47

2.6.1 *Drosophila melanogaster* life cycle 47

2.6.2 Microinjection 47

2.6.3 Characterization of transgenic lines 48

2.6.4 *Drosophila* genetics 50

APPENDIX A: General protocols 51

APPENDIX B: Stocks and solutions 55

APPENDIX C: Plasmids 59

3 RESULTS 61

3.1 Reticulon 61

3.1.1 Rtnl1 and atlastin display an antagonistic genetic interaction 61

3.1.2 Loss of Rtnl1 causes elongation of ER profiles 65

3.1.3 Rtnl1 overexpression induces shortening of ER tubules and loss of ER continuity 69

3.1.4 Rtnl1 has membrane fission activity *in vitro* 72

3.2 DP1 75

3.2.1 DP1 and atlastin interact genetically 75

3.2.2 *In vivo* analysis of DP1 function 78

4 DISCUSSION 83

5 REFERENCES 87

ABSTRACT

The endoplasmic reticulum (ER) is a complex membrane network that undergoes continuous remodeling while retaining its overall structure.

Drosophila atlastin localizes specifically to the ER and it has been demonstrated to be the GTPase responsible for the homotypic fusion of ER membranes. Recently it has been shown that atlastin interacts with other ER tubule-forming proteins such as reticulon and DP1/REEP/Yop1 families. These families show little overall sequence homology but they share a conserved domain of about 200 amino acids (Reticulon Homology Domain, RHD) that includes two hydrophobic segments that seems to form a hairpin in the membrane. The hydrophobic portions of these ER-shaping proteins appear to occupy the outer leaflet of the phospholipid bilayer, possibly generating curvature *via* hydrophobic wedging. Using *Drosophila melanogaster* we studied the function of reticulon (Rtnl1) and DP1 in maintaining and determining the morphology of the ER.

We found that in *Drosophila* Rtnl1 and atlastin interact genetically in an antagonistic manner and that modulation of Rtnl1 expression *in vivo* markedly affects atlastin loss and gain of function phenotypes. Indeed, we demonstrated that in *Drosophila* genetic elimination of Rtnl1 in the atlastin null background rescues the lethality associated with depletion of atlastin. This genetic interaction between Rtnl1 and atlastin is also supported by experiments in the *Drosophila* eye: ectopic expression of atlastin in the eye causes a small eye phenotype and RNAi mediated loss of Rtnl1 in an eye expressing atlastin results in enhancement of the atlastin dependent small eye phenotype. This antagonistic genetic interaction between Rtnl1 and atlastin suggests that these two proteins exert opposing functions in the control of ER architecture. Consistent with this hypothesis we found that loss of Rtnl1 leads to elongation of ER profiles while its overexpression produces shorter profiles. Moreover, FLIP experiments suggest that the ER lumen is discontinuous in *Drosophila* tissues overexpressing Rtnl1, further corroborating the hypothesis that Rtnl1 functions to counterbalance atlastin fusogenic activity by facilitating membrane fission to maintain the morphology of the ER. This activity was confirmed *in vitro* by showing that Rtnl1 reconstituted into giant unilamellar vesicles is sufficient to trigger membrane budding and production of vesicles.

Our studies of DP1 in *Drosophila* demonstrated that an antagonistic genetic interaction exists also between DP1 and atlastin. Indeed, such interaction is obvious both in the fly eye and in cell culture. Overexpression of DP1 in an eye simultaneously expressing atlastin resulted in a rescue of the atlastin-dependent phenotype and the hyperfusion phenotype caused by atlastin overexpression in COS-7 cells is rescued by coexpressing DP1. Moreover, we found that in *Drosophila* DP1 influences the morphology of the ER since neurons lacking DP1 display an elongation of the ER profiles. Thus, DP1 seems to have a function analogous to that of Rtnl1. This observation suggests that the membrane fusion mediated by atlastin is counterbalanced by the activity of two or possibly more proteins in order to maintain the general morphology of the ER network. Since it has been demonstrated that the RHD is the crucial region of reticulon and DP1, we propose that proteins containing this domain, such as reticulon and DP1/REEP/Yop1 proteins, could have an intrinsic ability to break ER membranes due to their capacity to induce extreme curvature of the lipid bilayers. Regions of extreme curvature can potentially be the sites of membrane scission because of the intrinsic instability of lipids. Our work suggests that a balance between membrane fusion and scission events is required to maintain the overall structure of the ER network and identifies potential candidate proteins with fission promoting activity.

RIASSUNTO

Il reticolo endoplasmatico (ER) è un organello altamente dinamico formato da un complesso sistema di membrane in continuo movimento e rimodellamento. La biogenesi ed il mantenimento dell'elaborata architettura dell'ER sono fondamentali per il corretto svolgimento delle sue funzioni e dipendono da eventi di fusione e di fissione delle membrane e dall'azione di proteine capaci di rimodellare le membrane. La fusione omotipica delle membrane dell'ER dipende dalla proteina atlastina, una GTPasi localizzata nelle membrane dell'ER. Al contrario, i meccanismi e le proteine coinvolte nella fissione delle membrane sono ancora sconosciuti. Recentemente, è stato dimostrato che atlastina interagisce con proteine appartenenti alle famiglie reticulons e DP1/REEP/Yop1, proteine coinvolte nel determinare la morfologia dell'ER. Queste proteine, sebbene appartenenti a famiglie differenti, posseggono un dominio altamente conservato di circa 200 aminoacidi (chiamato RHD) costituito da due domini transmembrana separati da una breve ansa citosolica. È stato proposto che le due porzioni idrofobiche si inseriscano nel foglietto esterno del doppio strato fosfolipidico in una struttura a forcina; tale struttura causerebbe quindi una deformazione del monostrato esterno della membrana, generando una curvatura localizzata della membrana.

In questa tesi, utilizzando come organismo modello *Drosophila melanogaster*, abbiamo studiato il ruolo delle proteine reticulon-1 (Rtnl1) e DP1 nel generare e mantenere la complessa architettura dell'ER.

Esperimenti *in vivo* hanno dimostrato che in *Drosophila* esiste una forte interazione genetica antagonistica tra Rtnl1 e atlastina. Infatti, i nostri risultati dimostrano che la letalità causata dall'assenza del gene atlastina è recuperata dalla simultanea perdita di funzione di Rtnl1. Questa interazione tra Rtnl1 e atlastina è stata confermata anche da esperimenti condotti nell'occhio di *Drosophila*: un'espressione ectopica di atlastina nell'occhio di *Drosophila* causa un occhio piccolo e rovinato; l'assenza di Rtnl1 in un occhio che contemporaneamente sovraesprime atlastina porta ad un peggioramento del fenotipo dell'occhio che diventa ancor più rovinato. Questa forte interazione genetica tra Rtnl1 e atlastina suggerisce che queste due proteine abbiano funzioni opposte nel mantenimento dell'architettura dell'ER. Inoltre, abbiamo dimostrato che l'assenza di Rtnl1 *in vivo* provoca l'allungamento dei profili dell'ER mentre, al contrario, la sua sovraespressione causa frammentazione e perdita della normale continuità del lume

dell'ER. Questi risultati avvalorano ulteriormente l'ipotesi che Rtnl1 sia in grado di controbilanciare l'attività di fusione mediata da atlastina probabilmente facilitando il processo di fissione delle membrane dell'ER. Questa ipotesi è stata confermata da esperimenti condotti *in vitro*: Rtnl1, infatti, è in grado di promuovere autonomamente il "budding" di membrana e la produzione di vescicole.

Abbiamo dimostrato che esiste una interazione genetica antagonistica anche tra DP1 e atlastina in *Drosophila*. Infatti, la sovraespressione simultanea di DP1 e atlastina nell'occhio porta ad un recupero del fenotipo "occhio rovinato" causato dall'espressione di atlastina. Inoltre, il fenotipo di iperfusione dell'ER causato dalla sovraespressione di atlastina in cellule COS-7 viene recuperato co-esprimendo DP1. Abbiamo anche dimostrato che DP1 è coinvolto nel mantenimento della morfologia dell'ER dato che neuroni privi di DP1 presentano profili dell'ER mediamente più lunghi rispetto a neuroni di controllo. DP1, quindi, sembra avere una funzione simile a quella di Rtnl1. Questi risultati suggeriscono che la fusione delle membrane dell'ER mediata da atlastina sembra essere controbilanciata dall'attività di due o più proteine che cooperano per mantenere la normale morfologia dell'ER. Dato che è stato dimostrato che il dominio RHD è la regione importante per la funzione di Rtnl1 e DP1, ipotizziamo che le proteine che contengono questo particolare dominio possano avere l'intrinseca abilità di rompere le membrane dell'ER. Questa abilità è dovuta alla capacità di queste proteine di indurre un'estrema curvatura delle membrane; a causa dell'intrinseca instabilità dei lipidi le regioni di estrema curvatura possono potenzialmente essere il punto di rottura delle membrane.

I dati da noi ottenuti suggeriscono che un equilibrio tra eventi di fusione e di fissione delle membrane sia necessario per mantenere la corretta morfologia dell'ER e identificano due proteine, Rtnl1 e DP1, che sono coinvolte nel promuovere gli eventi di fissione delle membrane dell'ER.

1 INTRODUCTION

1.1 Mechanisms of membrane fusion and fission

The biogenesis and maintenance of eukaryotic organelles is a complex and dynamic process that requires many protein and lipid components to generate the compartmentalization of function that is typical of the eukaryotic cell. In some cases, such as Golgi complex, proper organelle function depends upon communication between different compartments *via* vesicular transport. In other cases, such as mitochondria, organelle structure is highly dynamic, with membranes undergoing regular fission and fusion events, a process that is required for normal mitochondrial function (Moss *et al.*, 2011). Cellular membranes undergo continuous remodeling. Exocytosis and endocytosis, mitochondrial fusion and fission, entry of enveloped virus into host cells and release of the newly assembly virions, cell-to-cell fusion and cell division, and budding and fusion of transport carriers all proceed *via* topologically similar, but oppositely ordered, membrane rearrangements (Kozlov *et al.*, 2010).

Membrane fusion occurs when two initially separate and opposite membranes merge into one by undergoing a sequence of intermediate transformations that seem to be conserved between disparate biological fusion reactions. This membrane rearrangements begins with local merger of only the contacting monolayers of the two membrane, while the distal monolayers remain separate. The initial lipid bridge between the membranes is referred as the fusion stalk and signifies the first stage of fusion, called hemifusion. Stalk evolution ultimately leads to merger of the distal monolayers, resulting in the formation of a fusion pore that connects the volumes initially separated by the membranes and completes the membrane unification. The fusion pore must expand to a greater or smaller extend, depending on the specific biological context, for example, passage of small neurotransmitter molecules in the case of synaptic-vesicle exocytosis or a larger nucleocapsid in virus-cell fusion or to much larger nuclei in cell-to-cell fusion events.

Membrane fission – division of an initially continuous membrane into two separate ones – proceeds *via* the formation of a membrane neck, which is reminiscent of a fusion pore except that it narrows rather than expands. Theoretical analysis and experimental study demonstrate a scenario in which fission begins with self-merger of the inner monolayer of the neck membrane, which generates a fission stalk analogous to the fusion stalk.

Subsequent self-merger of the outer monolayer of the membrane neck completes the fission process.

The fundamentally common feature of fusion and fission in these pathways is the formation of a membrane stalk at an intermediate stage of the reaction, which is followed by stalk decay. Obviously, stalk formation requires transient disruption of the membrane structure and hence is opposed by the powerful hydrophobic forces working to maintain continuity and integrity of any lipid assembly. The evident distinction between fusion and fission is the reverse sequences of shapes adopted by the membranes and the opposite character of the overall topological transformation of the membrane surface. As result of fission, the membrane splits into two smaller ones that are, on average, more strongly bent and characterized by greater curvatures. By contrast, as result of fusion the merged membrane can partially relax the bending of the initial membranes by reducing the overall membrane curvature. Hence, the forces favoring membrane bending promote membrane fission, whereas the factors driving membrane unbending have opposite effect and support membrane fusion.

In addition, membrane self-connectivity changes in opposite directions as a result of fusion and fission. After fusion, the lipids and all membrane-bound molecules and molecular complexes can redistribute over the entire unified membrane area instead of being limited within one of the initial smaller membranes. By contrast, fission results in separation of one membrane into two unconnected membranes, thereby reducing the degree of membrane self-connectivity. Thus, the physical factors favoring membrane self-connectivity facilitate fusion, whereas fission is supported by forces that promote separation of the membrane surface into spatially disconnected compartments.

Membrane remodeling, either by fusion or fission, can occur if two physical requirements are fulfilled. First, the process must be energetically favorable overall. The system free energy before remodeling has to be higher than that after, meaning that remodeling must result in relaxation of the free energy. Second, the energies of the intermediate structures formed transiently in the course of remodeling and representing kinetic barriers must be low enough to be overcome by system thermal fluctuations within a biologically relevant time. Membrane remodeling is driven and controlled by proteins that provide the required energy. Thus, it must be considered how proteins can generate the conditions for bilayer remodeling by changing the structure and physical state of lipid bilayers (Kozlov *et al.*, 2010).

1.1.1 Proteins driving fusion

A common property of many proteins involved in endo- and exocytosis is their ability to strongly bend lipid bilayers (Graham & Kozlov, 2010). Accordingly, an attractive idea is that specialized proteins drive membrane fusion through the generation of membrane curvature. Proteins can generate membrane curvature *via* different mechanisms. These include induction of lipid asymmetry of the membrane bilayer by flippases and lipid-modifying enzymes, molding of the membrane surface by rigid protein scaffold, and insertion of hydrophobic protein domains into the lipid bilayers matrix. The latter is likely to be the most common mechanism that lies in expansion of the polar head region of one of the membrane monolayers by shallow insertions in its matrix of small hydrophobic or amphipathic protein domains (Kozlov *et al.*, 2010).

Several energy barriers have to be overcome for fusion to occur. One energetically demanding process is to bring about the close apposition of two membranes which requires protein clearance and the bringing together of repulsive membrane charges. The energy barriers related to curvature deformations during hemifusion-stalk and fusion-pore formation and expansion must also be overcome. The role of fusion proteins is to lower these barriers at the appropriate time and place to allow the regulation of the fusion process. Membrane fusion events generally require also molecules that locally disturb the lipid bilayers in order to reduce the energy barriers for fusion, and molecules that give directionality to the process. Moreover, the driving force for membrane fusion can come from many sources, for example from the energy derived from protein-protein interactions or from protein-lipid interactions, and ultimately these reactions will have been primed by ATP. Directionality might be achieved by fusion protein folding. In addition, curvature stress that promotes fusion-stalk formation will be relieved during fusion-pore opening and expansion, again giving directionality to the process from the beginning (Martens & McMahon, 2008). The different activities listed above do not have to be handled by different proteins, so the same molecules that promote hemifusion-stalk formation might promote fusion-pore expansion.

Membrane fusion between cells, viruses and cells, or transport vesicles and intracellular organelles employs distinct molecular machines.

1.1.2 Intracellular membrane fusion

Intracellular membrane fusion can either be heterotypic (when a membrane fuses with a dissimilar type of compartment; for example, synaptic vesicle exocytosis) or homotypic (when the same compartment fuses with itself; for example, mitochondrion-mitochondrion fusion). Much of what is known about intracellular membrane fusion has come from three major approaches: genetic studies in budding yeast, the study of the tightly regulated synaptic fusion machinery and identification of its core components, and lipid-mixing assays aimed at recapitulating the fusion reaction *in vitro*. These studies have led to the conclusion that most intracellular membrane fusion events are carried out by a largely conserved mechanism performed by the SNARE proteins and associated regulatory factors and effector proteins. The best studied process of SNARE-independent intracellular membrane fusion is mitochondrial homotypic fusion. It is a highly conserved process from yeast to humans. Observations from both yeast and mammalian cells have provided insights into the mechanism, establishing that the key players are members of the large GTPase dynamin-related protein family.

1.1.3 Mitochondrial membrane dynamics

Mitochondria are dynamic organelles that continually undergo fusion and fission. These opposing processes work in concert to maintain the shape, size, and number of mitochondria and their physiological function (Chan, 2012).

Mitochondrial fusion and fission processes are both mediated by large guanosine triphosphatases (GTPases) in the dynamin family that are well conserved between yeast, flies, and mammals. Their combined actions divide and fuse the two lipid bilayers that surround mitochondria (Youle & van der Bliek, 2012).

In mammals, three large GTPases are essential for mitochondrial fusion: the mitofusins Mfn1 and Mfn2 and OPA1. Depletion of any of these three GTPases results in severely reduced levels of mitochondrial fusion.

The mitofusins were the first proteins found to be important for mitochondrial fusion. They localize to the mitochondrial outer membrane where mediate fusion between mitochondrial outer membranes. They cause aberrations in mitochondrial morphology when overexpressed. Mouse embryonic fibroblasts (MEFs) lacking either Mfn1 or Mfn2 have highly fragmented mitochondria in contrast to the tubular network observed

in wild-type cells. Fusion assays indeed indicate a great reduction in the levels of mitochondrial fusion in single knockout MEFs and a complete loss of fusion in cells lacking both Mfn1 and Mfn2. When mitochondrial fusion rates are reduced, the mitochondrial population fragments into short tubules or small spheres because of ongoing mitochondrial fission in the face of less fusion. These observations support the idea that mitochondrial morphology is dictated by a balance between fusion and fission.

Fusion between mitochondrial inner membranes is mediated by a single dynamin family member called OPA1 (Optic Atrophy 1) in mammals (Youle & van der Bliek, 2012). Human genetic studies identified OPA1 as the gene mutated in the most common form of dominant optic atrophy, a disease in which retinal ganglion cells degenerate and cause atrophy of the optic nerve. Depletion of OPA1 results in severe mitochondrial fragmentation that is due to loss of mitochondrial fusion. Along with the loss of mitochondrial fusion, OPA1 deficiency leads to other cellular defects, including reduction and disorganization of cristae membranes, severely reduced respiratory capacity, and sensitivity to apoptosis.

The balance between the opposing processes of fusion and fission maintains the overall morphology of mitochondria and ensures that the mitochondrial population remains dynamic. Genetic and cell biological studies have identified DRP1, a dynamin-related protein, as the central player for mitochondrial fission. DRP1 is recruited from the cytosol to form spirals around mitochondria that constrict to sever both inner and outer membranes. Inhibition of DRP1 function, either by expression of a dominant-negative variant or RNA interference, results in very elongated mitochondria that entangle and collapse (Chan, 2012).

1.1.4 Proteins driving fission

During fission, bending energy accumulates owing to protein-driven narrowing of the membrane neck. It is thought that relaxation of this energy, resulting from splitting of the membrane neck into two separate membranes, drives fission (Kozlovsky & Kozlov, 2003). For some fission processes, the formation of a membrane neck seems to involve membrane scaffolding by protein complexes. For example, protein coats or scaffolds play an important role in the budding and release of newly assembled envelope viruses. A major role in this budding-fission process can be played by viral proteins that assemble under cell membranes. Assembly of a rigid protein coat on the membrane

surface can generate a membrane neck that emerges from the coat aperture. Continuous self-assembly of the coat, accompanied by closure of its aperture, results in narrowing of the membrane neck, accumulation of elastic stresses and ultimately in neck fission. Moreover, recent studies of protein-driven membrane rearrangements support the hypothesis that insertion of their amphipathic and small hydrophobic domains into the membrane matrix constitutes the major factor used by many proteins, including the BAR-domain proteins and dynamin family proteins, for membrane fission (Kozlov *et al.*, 2010).

1.1.4.1 BAR domains

The hydrophobic insertion mechanism assumes the partial embedding into the membrane matrix of hydrophobic or amphipathic protein domains. An integral trans-membrane domains spanning the whole membrane also bend membrane, if it had an asymmetric cone -or inverted cone- like shape or an oblique intra-membrane orientation. More biologically relevant appear to be small protein domains embedding only shallowly into the upper part of a lipid monolayer. Most frequently, such domains are represented by amphipathic alpha-helices, penetrating the membrane to the depth of about 40% of a monolayer thickness (Kozlov *et al.*, 2010).

BAR (Bin–Amphiphysin–Rvs) domains are modules that sense membrane curvature (McMahon & Gallop, 2005). All BAR proteins are composed of a helix bundle, where three helices of one monomer form into a dimer, producing a six-helix bundle that display various degrees of intrinsic curvature. In BAR domains, the positively charged residues are enriched at a particular surface of the dimer, identifying it as the membrane contact sites. Considering only the dimer of the BAR domains, most BAR domains are thought to fit with negatively charged lipid membranes through their positive concave face. Furthermore, they induce membrane tabulation *in vitro* (Suetsugu *et al.*, 2014). Most BAR proteins have at least one additional domain, such as a src-homology 3 (SH3) domain, which enables BAR proteins to interact with proline-rich domain (PRD) containing proteins. Thus, BAR domain proteins are scaffolding proteins that organize a variety of other proteins in a curvature-dependent manner. BAR domains are also frequently found in combination with N-terminal amphipathic helices (N-BAR domains). The amphipathic helix, in combination with the concave structure, is important for the ability of the BAR domains to sense and induce membrane curvature.

Indeed, insertion of NH_2-terminal amphipathic helices into membranes causes changes in lipid packing and effectively creates local membrane curvature. Thus, the NH_2-terminal amphipathic stretch plays pivotal roles in membrane tabulation and shallow helical fold insertion into the membranes (Mim & Unger, 2012). Thus, membrane fission in this system should be driven by the mechanism by which N-BAR generates membrane bending, the hydrophobic insertion mechanism.

1.1.4.2 Dynamin protein

Recent studies suggest that the hydrophobic insertion mechanism also plays a primary role in dynamin-mediated fission. Dynamin is a large multidomain GTPase that assembles into helical arrays around the necks of deeply invaginated clathrin-coated pits and catalyzes membrane fission during the final stages of endocytosis (Chappie & Dyda, 2013). Dynamin contains a G domain that binds and hydrolyses GTP, a stalk domain that promotes self-assembly, a pleckstrin homology (PH) domain and a PRD. These unique domains almost certainly convey the specific function of dynamin in the cell. The PH domain preferentially binds phosphatidylinositol 4,5-biphosphate (PIP_2), a lipid enriched in the plasma membrane, which is believed to function as a key signaling molecule for the recruitment and assembly of the clathrin machinery. The PRD provides a platform for dynamin partners to bind *via* SH3-binding motifs (Sundborger & Hinshaw, 2014).

Dynamin was the first protein shown to possess membrane tubulation activity when mixed with liposomes. Because the characteristic helical pattern seen on the tubes matched the dimension of the dynamin oligomer formed in the absence of membrane, it was proposed that dynamin deforms the membrane by forming a scaffold. However, at low concentrations of dynamin, a competition between the polymerization energy of dynamin and the energy required to deform the membrane leads to the membrane curvature-dependent nucleation of dynamin (Roux, 2014).

The discovery of dynamin self-assembly into helical structures on membrane surfaces and conformational changes of dynamin oligomer upon GTP hydrolysis have stimulated a series of mechanochemical models of dynamin action. These models propose that the formation of helical dynamin oligomers scaffolds the membrane into a cylindrical shape, which loses its stability and undergoes fission as a result of narrowing and/or

stretching of the dynamin helix resulting from GTP hydrolysis and/or detachment of GDP-dynamin from the membrane surface (Bashkirov *et al.*, 2008).

1.2 Endoplasmic reticulum

1.2.1 ER structure and organization

The endoplasmic reticulum (ER) is arguably the most complex, multifunctional organelle of eukaryotic cells. It plays critical roles in the synthesis, modification, quality control, and trafficking of integral membrane proteins and soluble proteins destined for secretion, the mobilization and regulated release of Ca^{2+}, sterol/lipid synthesis and distribution, signalling, carbohydrate metabolism, and detoxification of harmful substances. Reflecting these diverse functions, the ER comprises a continuous membrane system that include the inner and outer membranes, sheet-like cisternae, and a network of interconnected tubules extending promiscuously into the cell periphery. The ER is the largest continuous organelle, with its membranes comprising about half of the total membrane and its lumen enclosing about 10% of the volume of a typical eukaryotic cell (Goyal & Blackstone, 2013). Some ER domains are obvious and can be distinguished by their shapes using fluorescence microscopy. These include the nuclear envelope (NE) and the cytoplasmatic cisternae and tubules that form the interconnected peripheral ER. The NE is a distinct domain of the ER comprised of two large, flat membrane bilayers, the inner and outer membranes (INM and ONM respectively). The INM and ONM are separated by the perinuclear space, but are connected to each other at nuclear pores (Voeltz & Friedman, 2011). The peripheral ER is a network of interconnected tubules that extends throughout the cell cytoplasm (Terasaki and Jaffe, 1991). At the ultrastructural level it can be divided into two types, smooth ER (SER) and rough ER (RER). The RER has a sheet-like morphology and is characterized by the presence of ribosomes associated with the biosynthesis of secretory and membrane proteins. Conversely, the SER is devoid of ribosomes and tends to be more tubular in structure and is involved in lipid synthesis and delivery (Chen *et al.*, 2013). The smooth ER also includes zones of contact with membranes of other organelles. A subdomain morphologically and functionally distinct from the surrounding smooth ER is the transitional ER, where proteins and lipid from the ER are exported through COPII coated vesicles towards the secretory pathway (Pendin *et al.*, 2011a).

1.2.2 The ER is a single compartment

Several approaches have provided evidence that the ER is a single membrane system with a continuous intralumenal space. In one experiment, a fluorescent dye that cannot exchange between discontinuous membranes was injected into cells in an oil droplet. The dye diffused throughout the cell in a membrane network that, based on morphological criteria, was the ER. This was observed in a number of different cell types including sea urchin eggs (Terasaki and Jaffe, 1991) and Purkinje neurons (Terasaki *et al.*, 1994). Because the dye spread in fixed as well as live cells it must be diffusing through a continuous network rather than being transported by active trafficking.

The continuity of ER membranes network was also proved by fluorescence loss in photobleaching (FLIP). In this experiment, GFP-tagged proteins are targeted either to the lumen or membrane of the organelle, and then a small region of the labelled membrane is continuously bleached using the beam from a confocal laser scanning microscope. If membranes are interconnected, unbleached fluorescent molecules diffuse into the illuminated spot where they are bleached; eventually, the fluorescence of the entire organelle is depleted. When FLIP experiments were performed on ER membranes, all fluorescence was rapidly lost from the entire membrane network (Dayel & Verkman, 1999), indicating the continuity of the ER membrane system.

1.2.3 Propagation of the ER during mitosis

All components of the cell are dramatically rearranged during cell division. The ER/NE membranes undergo structural and functional changes during mitosis to allow redistribution of this organelle and its associated proteins to daughter cells. Accumulating evidence suggests that the ER network does not disassemble into vesicles during the cell cycle, but that it is divided between daughter cells by cytokinesis. The strongest support for maintenance of ER continuity comes from FLIP experiments demonstrating that ER markers retain interphase patterns of motility during mitosis (Ellenberg *et al.*, 1997). In addition, both light and electron microscopy show that ER networks can be visualized during cell division (Koch & Booth, 1988; Ellenberg *et al.*, 1997; Terasaki, 2000).

In animal cells, the NE membrane fragments and the membrane and its associated proteins are absorbed into the peripheral ER, which does not disassemble to a significant degree in most cells. While the peripheral ER remains continuous during transitions between interphase and mitosis, the shape does not change from a mixture of sheets and tubules in interphase to a highly reticulated tubular ER structure devoid of sheets during mitosis. This change in peripheral ER structure during mitosis is accompanied by some measured changes in ER function. It has been shown that both ER exit site numbers and ribosome density are reduced, suggesting that ER-dependent translation and protein transport are also presumably reduced if not halted (Puhka *et al.*, 2007). A highly reticulated tubular ER may be more evenly redistributed that sheets to daughter cells at the end of mitosis in animal cells. In addition, recent evidence suggests that the structure of the peripheral ER network during mitosis can affect the rate of NE reformation around chromatin. Using *in vitro* system derived from *Xenopus* egg extracts, live-imaging showed that an intact tubular network first binds to chromatin to initiate NE formation. When tubular ER formation was inhibited NE formation was also inhibited (Anderson & Hetzer, 2008).

1.2.4 ER dynamics

The ER continuously undergoes significant rearrangements of its structure: vesicles bud from and become incorporated into the ER membrane, new tubules form from existing ones, tubules retract, sheets transition to tubules and tubules to sheets, tubules fuse and likely break apart. Remarkably, despite this constant reorganization the ER maintains luminal continuity and its characteristic structure. All these events contribute to making the ER a highly dynamic organelle. Different mechanisms underlie the different modalities of ER dynamics. The outgrowth and retraction of tubules depend on the close association between the ER and the cytoskeleton; shape to shape transition of the ER membrane are determined by the ability of specific proteins to distort phospholipid bilayers; finally, ER membranes are remodeled through fusion and, probably, fission processes.

Like many other organelles, the ER has a close relationship with the cytoskeleton, which has been proposed to provide the driving forces for ER movement and morphological transitions. In animal cells, microtubules play a major role in ER remodeling. Treatment with nocodazole, a microtubule disassembly reagent, causes

dramatic changes in ER morphology (Bannai *et al.*, 2004; Shibata *et al.*, 2009). Microtubule-based ER dynamics were studied with time-lapse microscopy and appear to be based on two different mechanisms. First, ER-associated motor protein mediates ER sliding along the existing microtubule (MT); second, the attachment of the ER membranes on the growing tips of microtubules through tip attachment complexes (TAC) allows the extension of ER tubules (Waterman-Storer & Salmon, 1998). During TAC movements, the tip of the ER tubule is bound to the tip of a dynamic MT, and the new ER tubule grows in a motor-independent way in concert with the dynamics of the plus-end of the MT. TAC events occur through a complex between the integral ER membrane protein STIM1 and a protein that localizes to the tip of a dynamic MT, EB1 (Grigoriev *et al.*, 2008). During ER sliding events, tubules are pulled out of the ER membrane by the motor proteins kinesin-1 and cytoplasmic dynein along MTs that are marked by acetylation. ER sliding is much more common than TAC and is the predominant mechanism responsible for dynamic ER rearrangements in interphase cells (Friedman *et al.*, 2010). The difference between TAC and ER sliding mechanisms suggest that they might contribute to different ER functions.

In yeast and plants, the actin cytoskeleton, rather than the microtubule network, is required for ER dynamics (Prinz *et al.*, 2000).

The cytoskeleton contributes to ER dynamics, but it is not necessary for the maintenance of the existing ER network. Although depolymerization of microtubules by nocodazole in mammalian tissue culture cells inhibits new tubule growth and causes some retraction of ER tubules from the cell periphery, the basic tubular-cisternal structure of the ER remains intact (Terasaki *et al.*, 1986). Similarly, actin depolymerization in yeast blocks ER movements but does not disrupt its structure (Prinz *et al.*, 2000).

1.2.4.1 Membrane shape and shape transition

ER domains and their membrane shape are generally fluid and change during processes such as cell division, growth and metabolic state. The different domains within the ER membrane exhibit notable morphological variation which depends on the spatial arrangement of the lipid bilayers in low curvature sheets or high curvature tubules indicating that membrane shaping relates to the generation of membrane curvature (Zimmerberg & Kozlov, 2006). A complex interplay of factors is likely to ultimately

determine membrane morphology, however, one important way to shape membranes involves the use of proteins able to deform lipid bilayers. Proteins can shape the membranes in a variety of ways. Mechanical force can be applied to a lipid bilayer by molecular motors pulling on the membrane proteins. Peripheral membrane proteins with an intrinsic curvature can conform membranes on their shape and integral membrane proteins with specialized hydrophobic domains can selectively insert into the outer monolayer to physically generate curvature (Shibata *et al.*, 2009). All these mechanisms could synergistically contribute to conferring the typical shape of the ER domains. However, it has been proposed that the reticulon and DP1/REEP/Yop1 proteins, that are two classes of highly conserved, integral membrane proteins, are predominantly involved in the morphogenesis of the peripheral ER tubules (Voeltz *et al.*, 2006; De Craene *et al.*, 2006). Their topology is thought to contribute to their ability to deform the membrane. Their depletion in yeast and mammalian cells converts the peripheral ER tubules into sheets while their overexpression converts peripheral ER sheets into tubules (see Introduction 1.4; Shibata *et al.*, 2008; Voeltz *et al.*, 2006).

In contrast to tubule formation, the mechanisms utilized to produce and stabilize the sheet-like morphology of ER cisternae are less well understood. It has been shown that reticulon and DP1/REEP/Yop1 segregate into the tubular ER regions but are essentially excluded from the NE and scarce in peripheral ER sheets, suggesting that their absence may prevent them from assuming a tubular morphology (Voeltz *et al.*, 2006) Among the mechanisms believed to be responsible for maintenance of sheet morphology are the presence of polyribosomes complexes. Indeed, stripping the ER of ribosomes with puromycin results in cells with a greater proportion of tubules compared to untreated cells (Puhka *et al.*, 2007) and overexpression of the membrane ribosome binding protein p180 leads to an increase in rough ER sheets (Benyamini *et al.*, 2009). Another hypothesis proposes that the flat shape of ER sheets depends on scaffolding within the ER lumen by proteins like coiled-coil protein CLIMP63. Oligomers of CLIMP63 bound to membrane and spanning the ER lumen may determine the thickness of ER sheets. However, reticulon and DP1/REEP/Yop1 appears to be involved in the formation of the ER sheets. Because these proteins can localize to sheet edges their oligomerization may generate scaffolds around curved membranes, which may be shaped as open arcs, whose function would be to stabilize the high membrane curvature at the edges. Thus, a theoretical model has been developed supporting the view that reticulon and

DP1/REEP/Yop1 alone can generate both tubules and sheets, and suggesting that their abundance determines the ratio of these domains (Shibata *et al.*, 2008).

1.2.4.2 Fusing the ER network

Another critical aspect of ER dynamics is membrane fusion. When observed *in vivo* by GFP labelling, the ER undergoes obvious fusion events that are visible as the merging of separate tubules. Membrane fusion activity is essential for preserving the typical structure of the ER (Vedrenne & Hauri, 2006). Indeed, it has been demonstrated that a fusion reaction is absolutely required for ER network formation using an *in vitro* system derived from *Xenopus* egg extracts (Dreier & Rapoport, 2000).

Three-way junctions are key elements of the ER network. They are formed when the tip of an ER tubule fuses to the side of another tubule, forming a new polygon within the network. Two parallel studies revealed that atlastin, a dynamin-like GTPase, is a critical mediator of homotypic ER fusion (see Introduction 1.3; Hu *et al.*, 2009; Orso *et al.*, 2009). Consistent with its role in ER tubule fusion, atlastin displays a punctuate distribution along ER tubules and is enriched at three-way junctions (English & Voeltz, 2013). Anti-atlastin antibodies were shown to inhibit ER network formation *in vitro*, suggesting a critical role for this protein in shaping the ER (Hu *et al.*, 2009). Orso and colleagues provided the first evidence that *Drosophila* atlastin is sufficient to catalyze membrane fusion *in vitro*. *In vivo* depletion studies in *Drosophila* neurons revealed that the loss of atlastin causes discontinuity of the ER lumen and fragmented ER network (Orso *et al.*, 2009), whereas overexpression of a GTPase deficient form of atlastin leads to long unbranched ER tubules in mammalian cells (Hu *et al.*, 2009).

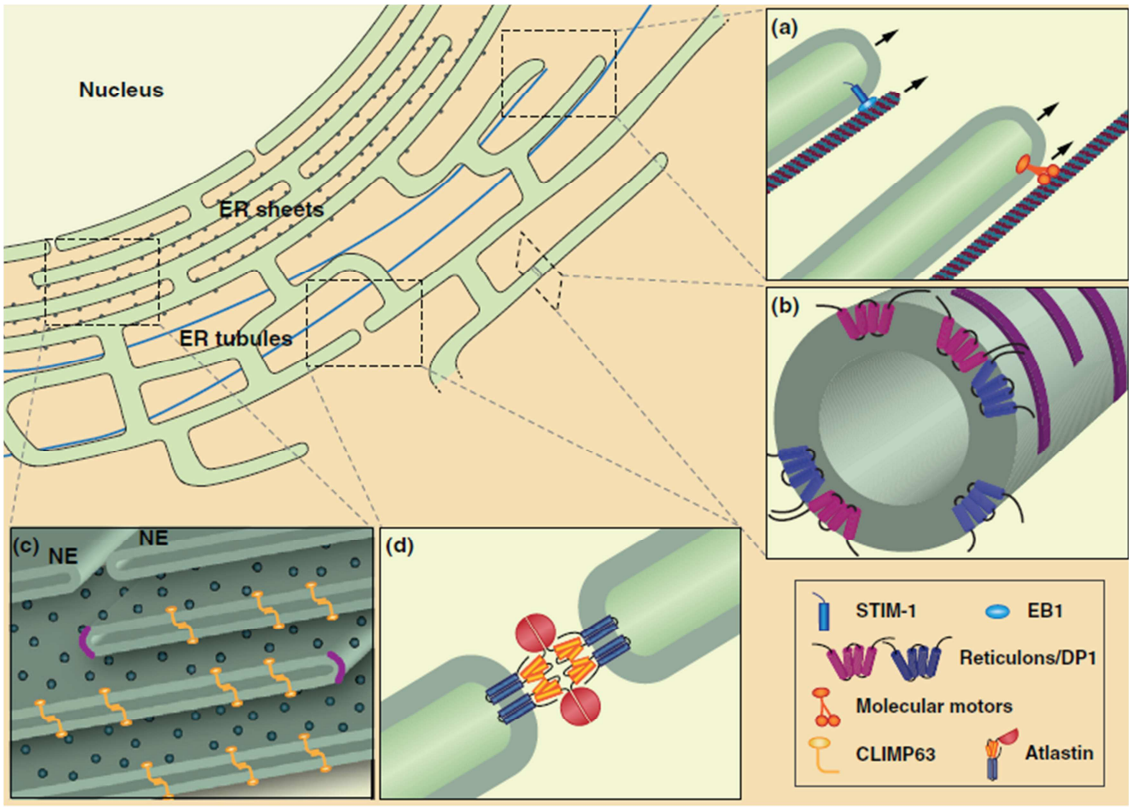

Fig. 1 – Domain organization of the endoplasmic reticulum network within the cell. (**a**) ER tubules move about the cytoplasm by attaching to microtubules using a TAC mechanism (left) or by a sliding mechanism (right). (**b**) The reticulons and DP1/REEP/Yop1 shape flat membranes into tubules using a combined wedging and scaffolding mechanism. Their hydrophobic segments insert like a wedge in the outer lipid layer causing the bilayer to bend and their ability to homo- and hetero-oligomerize may produce arc-like scaffolds around the tubules. (**c**) ER sheets, observed here in cross section, can be generated by the presence of the reticulons and DP1/REEP/Yop1 at their edges to stabilize locally the high curvature. In addition, transmembrane scaffolding proteins localized in both membranes interact through their luminal domains to maintain the two membranes flat and at a constant distance. NE, nuclear envelope. (**d**) Two ER tubules in the process of being merged by the fusogenic activity of the atlastin GTPase (Pendin *et al.*, 2011).

1.3 Atlastin

1.3.1 SPG3A gene

The SPG3A gene is localized on chromosome 14 and encodes a 558 amino acid protein named atlastin-1. SPG3A gene is a member of a larger family of genes that are responsible for a group of inherited neurological disorders called Hereditary Spastic Paraplegia (HSP). HSP is a progressive spastic weakness of the lower extremities due to the degeneration of axons in corticospinal motor neurons at their distal ends. Mutations in the SPG3A gene were identified for the first in HSP patients in 2001 (Zhao *et al.*,

2001). So far, 40 mutations have been reported in atlastin-1, most of which cause early-onset pure autosomal-dominant HSP by haploinsufficiency (Fassier *et al.*, 2010).

1.3.2 Atlastin subfamily

In humans there are two other atlastin family members, named atlastin-2 and -3. This division is conserved in a variety of rodents and higher mammals. However, some species such as *Drosophila melanogaster*, *Caenorhabditis elegans*, and the sea urchin express only one atlastin, indicating that the three atlastins in higher species may have at least partially overlapping functions.

Atlastin -2 and atlastin-3 are highly similar structurally to atlastin-1: they are transmembrane proteins with N- and C- terminals facing the cytoplasm and they are capable of oligomerization (Rismanchi *et al.*, 2008).

1.3.3 Atlastin structure

Atlastin-1 protein presents a N-terminal GTPase domain that contains the four canonical GTP binding motifs of large GTPases (Praefcke & McMahon 2004). Based on the high similarity of the GTPase domain, atlastin-1 has been included in the dynamin family of large GTPases. After the GTPase domain the protein presents a midportion (three-helix bundle, 3HB), two transmembrane (TM) domains and a short C-terminal tail (CT). Atlastin-1 is an integral membrane protein with both the N-terminal GTP-binding and the C-terminal domains exposed to the cytoplasm (Zhu *et al.*, 2003).

In an effort to understand the atlastin-associated fusion machinery, three crystal structures of the N-terminal cytosolic domain (residues 1-446) of human atlastin-1 have been determined (Bian *et al.*, 2011; Byrnes & Sondermann, 2011). In all three forms of atlastin-1, the molecule forms a dimer with the GTPase domains facing each other, but the position of the 3HB differs. In form 1, atlastin-1 is in complex with GDP, the two 3HBs associate with the paired GTPase domains and form a crossover conformation. In this case, the connecting TMs would have to sit in the same membranes; thus, the structure corresponds to a “post-fusion” state in which the membranes have already fused. In form 2, atlastin-1 is also GDP-bound, but in the presence of high concentration of inorganic phosphate. The two 3HBs associate with their own GTPase domains and point in opposite directions. This structure implies that two atlastin molecules likely sit

in opposing membranes, corresponding to a membrane-tethered “pre-fusion” state. In form 3, atlastin-1 is crystallized with either GDP/AlF_4 or GppNp. The two 3HBs come even closer than in form 1 (Byrnes *et al.*, 2013). Collectively, atlastin-mediated fusion requires dimerization resulting from GTP binding and conformational changes induced by GTP hydrolysis (Bian *et al.*, 2011; Byrnes & Sondermann, 2011; Lin *et al.*, 2012). In addition to the N-terminal cytosolic domain, the TM and CT have also been shown to play important roles in fusion. The TM of atlastin-1 appears to be more than a membrane anchor, as deletion or replacement of the TM region results in a loss of fusion activity. The CT of atlastin forms an amphipathic helix that binds and destabilizes the membranes to facilitates fusion (Liu *et al.*, 2012).

Recently, Saini and colleagues used membrane-anchored atlastins in assays that separate tethering from fusion to dissect the requirement for each. They found that tethering depended on GTP hydrolysis, but, unlike fusion, it did not depend on cross-over. Thus, GTP hydrolysis initiates stable head-domain contact in trans to tether opposing membranes, whereas cross-over formation plays a pivotal role in powering the lipid rearrangements for fusion (Saini *et al.*, 2014).

1.3.4 Human atlastins

The atlastin-1 protein is most abundant in brain, although it is also present at lower levels in other tissues, including lung, smooth muscle, adrenal gland, kidney, and testis. Within the brain, atlastin-1 is prominently enriched in the lamina V pyramidal neurons in the cerebral cortex (Zhu *et al.* 2003). The subcellular localization of atlastin-1 is controversial: the protein has been reported to localize to either Golgi (Zhu *et al.* 2003; Namekawa *et al.* 2007) or endoplasmic reticulum membranes (Namekawa *et al.* 2007). Atlastin-1 has also been reported to be enriched in vesicular structures within axonal growth cones and varicosities as well as at axonal branch points in cultured cerebral cortical neurons (Zhu *et al.*, 2006).

Atlastin-2 and atlastin-3 are expressed at higher levels in peripheral tissues and much less in the brain (Zhu *et al.*, 2003; Rismanchi *et al.*, 2008; Farhan & Hauri, 2009). At the subcellular level, atlastin-2 and atlastin-3 show prominent localization to the endoplasmic reticulum (Rismanchi *et al.*, 2008).

Overexpression of wild-type atlastin-1 resulted in the formation of aberrant sheet-like structures; instead overexpression of wild-type atlastin-2 or -3 did not noticeably affect

ER morphology as seen by light microscopy, but produced a fragmented Golgi. However, overexpression of GTPase-deficient mutants of atlastin-1-3 resulted in more elongated and tubular ER with less branching, as well as a fragmented Golgi. These effects might be a result of a dominant-negative effect of the overexpressed protein. Overexpression of either wild-type or mutant atlastins did not significantly affect protein trafficking (Rismanchi *et al.*, 2008; Farhan & Hauri, 2009).

1.3.5 *Drosophila* atlastin

The *Drosophila* genome contains a single highly conserved atlastin-1 ortholog: D-atlastin (D-atlastin maps to the 96A13 band of the third chromosome). D-atlastin is 541 amino acids long and has a predicted molecular mass of 61 kDa. The D-atlastin sequence is highly homologous with all three human isoforms, ranging between 44% and 49% identical (61% and 68% similar) over the entire length of the protein (Moss *et al.*, 2011). *Drosophila* and human atlastins show remarkable homology and conservation of domain organization. Immunohistochemistry experiments showed that D-atlastin is ubiquitously expressed, and its expression levels are high during embryonic development (Orso *et al.*, 2009).

In vivo and *in vitro* analyses provide strong evidence that D-atlastin is the vital GTPase required for homotypic fusion of ER membranes. In response to loss of D-atlastin, the ER network becomes fragmented. D-atlastin is capable of homo-oligomerization and self-association can occur within the same membrane as well as between opposing membranes. This property leads to the formation of trans-complexes that tether adjacent ER membranes. *In vivo* overexpression of D-atlastin results in the expansion of ER elements, consistent with excessive membrane fusion. In agreement with *in vivo* experiments, recombinant atlastin potently drives membrane fusion *in vitro* in a GTP-dependent manner. D-atlastin requires GTPase activity to exert its function because GTPase-deficient atlastin (K51A) is functionally inactive *in vivo*, fails to tether ER membranes owing to its inability to homo-oligomerize, and does not promote membrane fusion *in vitro* (Orso *et al.*, 2009).

The structure of the N-terminal cytoplasmic domain of human atlastin-1 was solved by X-ray crystallography in two recent studies. Molecular modeling approach indicates that the N-terminal cytosolic region of D-atlastin is highly likely to adopt a conformation similar to that observed for atlastin-1. In particular, the middle region contains the

predicted α-helix and its sequence is compatible with folding as a three-helix bundle (Pendin *et al.*, 2011b).

The structure-function studies of D-atlastin have led to develop a working model of atlastin function in membrane fusion. The fusion cycle begins with nucleotide-free atlastin monomers in opposing ER membranes. Then the nucleotide binding results in a permissive state for association between the GTPase domains. The interaction between GTPase domains matures to a more stable dimer facilitated primarily by an interaction between the middle domain three-helical bundle segments. This conformational change is achieved, perhaps driven by nucleotide hydrolysis, by rotating the GTPase domain dimer 180 degrees which forces the three-helix bundles into close proximity. The new association between adjacent 3HBs liberates the C-terminal tail domain to perform its required role. The activity of this C-terminal domain may be accomplished by forming a new association with the dimeric 3HB or by direct interaction with lipid. An interaction between the membrane surface and the amphipathic C-terminal tail could destabilize the bilayer and provide the driving force for outer leaflet mixing, resulting in a hemifusion intermediate that resolves by inner leaflet mixing to full fusion. Finally, the GDP release could then promote dissociation (Fig. 2; Moss *et al.*, 2011).

It is also possible that an interaction between the 3HBs of opposing atlastin molecules occurs during the nucleotide-dependent conformational change. It seems that the 3HB plays a minor or negligible role in the nucleotide-independent oligomerization of atlastin molecules, rather, the trans-membranes mediate this association of atlastin molecules in the same membrane before nucleotide binding (Liu *et al.*, 2012).

Recently, studies performed in our laboratory reveal important mechanistic insights into the functional properties of D-atlastin and suggest a model for atlastin-mediated homotypic fusion of ER membranes. Our hypothesis, that differs from the interpretation of the structural data on atlastin-1 which suggest that dimerization occurs through the GTPase domain, is that stable D-atlastin dimerization requires the 3HB domain. In our hypothesis, upon nucleotide binding, D-atlastin inserted within the ER membrane undergoes a conformational change that reorients the 3HB, making it available for interaction with the 3HB from a similarly primed atlastin molecule. Formation of a trans-complex induced by assembly of the 3HBs pulls the two membranes into very close apposition. The energy released after GTP hydrolysis is transduced to the lipid bilayers, resulting in their destabilization. The combination of close proximity and

membrane destabilization then drives the fusion reaction. Release of the nucleotide could lead to complex disassembly, and another cycle would be prompted by binding of a new GTP molecule. In this model of membrane fusion the GTP binding is used to drive a conformational rearrangement that promotes membrane tethering and the chemical energy of GTP hydrolysis to merge opposing phospholipid bilayers.

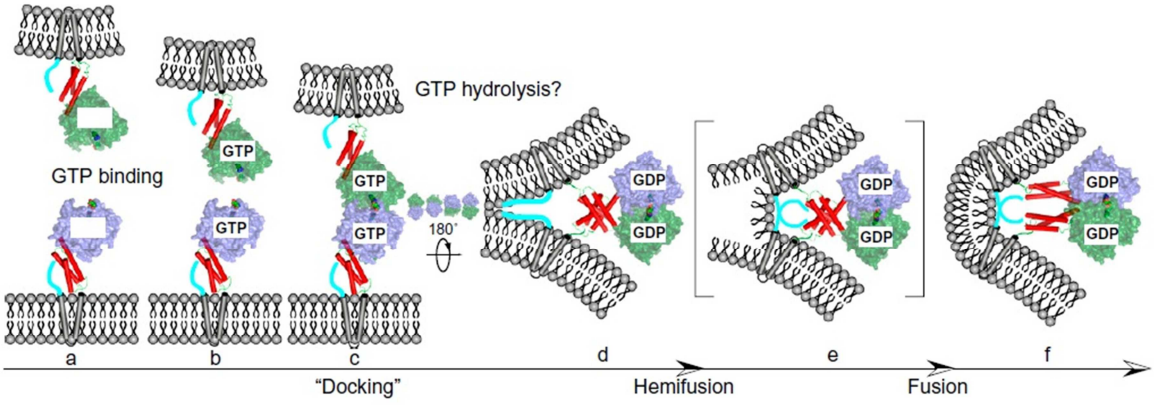

Fig. 2 – Model for atlastin-mediated fusion. The GTPase domains are cartooned as surface representations, the middle domains are shown as red cylinders, the transmembrane domains are illustrated as gray cylinders, and the C-terminal tails are shown as thick cyan lines. (**a**) Bilayer containing nucleotide-free prefusion monomers. (**b**) GTP-bound prefusion monomers. (**c**) Initial, unstable docking intermediate between GTP-bound monomers through surfaces on the GTPase domain. (**d**) Stabilized dimer formed by domain rotation and 3HB interaction resulting from GTP hydrolysis. (**e**) Putative hemifusion intermediate. (**f**) Postfusion bilayer (Moss *et al.*, 2011).

1.4 Reticulon and DP1

1.4.1 Reticulon and DP1 family

The reticulons are a recently discovered family of proteins that derive their name from their predominant localization to the membrane of the endoplasmic reticulum (van de Velde *et al.*, 1994). The reticulons were originally identified as a markers for carcinomas with neuro-endocrine characteristics; subsequently reticulons have been identified in all eukaryotic organisms studied to date including yeast, plants and fungi, suggesting an evolutionary conserved role for these proteins in the eukaryotic cell (Oertle *et al.*, 2003). All family members contain the reticulon homology domain (RHD), a conserved region at the carboxy-terminal end of the molecule consisting of two hydrophobic regions flanking a hydrophilic loop. Nearly all reticulon genes contain multiple introns and exons and most are alternatively spliced into multiple isoforms. Intron losses and gains over the course of evolution have given rise to the large, diverse reticulon family. Across phyla, the second hydrophobic region of the RHD is the most highly conserved, followed by the first hydrophobic region, with the carboxyl terminus at least conserved. In mammals, there are four reticulon genes encoding reticulon proteins RTN1-4. The RHDs of RTN1, 3 and 4 share the highest sequence identity at the amino-acid level (average 73%), whereas RTN2 has only 52% identity with human RTN4 (Yang & Strittmatter, 2007). Mutation in RTN2 (codified by SPG12), like insertion, deletion and substitution, are associated with autosomal dominant uncomplicated HSP (Montenegro *et al.*, 2012) while missense mutation in RTN4 are implicated in schizophrenia (Lazar *et al.*, 2011).

The other family related to the reticulon family consists of the DP1/REEP/Yop1 proteins, which includes six mammalian DP1/REEP genes and the yeast ortholog Yop1p (Hu *et al.*, 2008; Hu *et al.*, 2009). The reticulons interact with DP1 (Deleted in Polyposis) or REEP5 in mammals and Yop1p in *Saccharomyces cerevisiae* (Voeltz *et al.*, 2006). The DP1/REEP/Yop1 family is again ubiquitous. Although not sequence related to the reticulons, these proteins also contain a conserved domain with two hydrophobic hairpins in the membrane (Hu *et al.*, 2011).

1.4.2 Reticulon and DP1 structure

The reticulons do not share any primary sequence homology with member of DP1/REEP/Yop1 family. However, both families have a conserved domain of about 200 amino acids containing two long hydrophobic segments (Shibata *et al.*, 2008). Indeed, a key feature of the RHD is the presence of two unusually long hydrophobic regions, each 28-36 amino acids long, which are thought to be membrane-embedded regions, separated by a hydrophilic loop of 60-70 amino acids, and followed by a short carboxy-terminal tail of about 50 amino acids. Although much amino acid identity has been lost over the course of evolution, the overall structure of the RHD has been preserved from plants to yeast to humans. This suggests that three-dimensional protein structure is of greater importance than individual residues for RHD function (Yang & Strittmatter, 2007). Moreover, RHD hydrophobic regions are unusually long, in comparison to the alpha-helix domain of typical transmembrane proteins that are only about 20 amino acids in length. Therefore, the topology of these hydrophobic regions within membranes diverges from the usual integral membrane proteins. The reticulon and DP1 transmembrane domains do not fully cross the membrane but each of them forms a hairpin-like structure into the outer leaflet of the lipid bilayer with both N- and C-terminal ends facing in the cytosolic side ("W" topology; Shibata *et al.*, 2008).

The particular RHD length is a required domain for reticulon and DP1/REEP/Yop1 partitioning and interactioning in the ER membrane. Using fluorescence recovery after photobleaching, it has been revealed that mammalian reticulons and DP1, like their yeast homolog, are less mobile in the membrane than normal ER proteins. This slow diffusion is probably not caused by their tethering to the cytoskeleton. Rather, immobility appears to be caused by their oligomerization that is evident in sucrose gradient centrifugation and cross-linking experiments. The conserved RHD containing the two hydrophobic segments is sufficient for reticulon oligomerization. This conclusion is supported by the isolation of mutants of yeast Rtn1p that have amino acid changes in the RHD; they oligomerize less extensively according to sucrose gradient sedimentation experiments, and they diffuse rapidly in the membrane. The same mutants also no longer localize exclusively to the tubular ER, suggesting that oligomerization of the reticulons and DP1/REEP/Yop1 is required for their proper localization (Shibata *et al.*, 2008).

In contrast to the closely conserved C-terminal domain, the N-terminal regions show little or no sequence homology. These variable domains are likely to interact with distinct proteins and to confer specific biological functions to the various reticulon isoforms (Di Sano *et al.*, 2012).

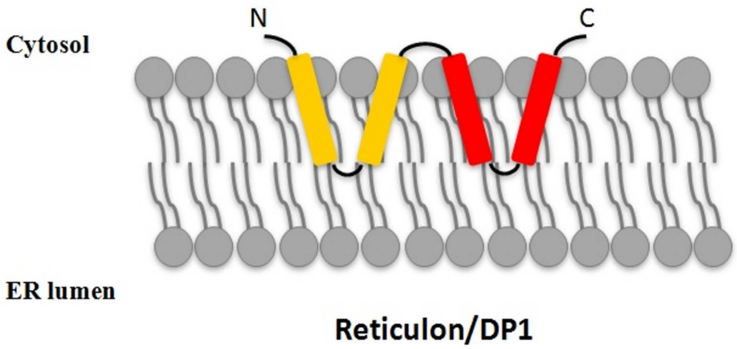

Fig. 3 – Reticulon and DP1 structure. Reticulon and DP1 proteins contain large hydrophobic segments that are longer than conventional α-helical transmembrane domains. Zurek *et al.* (2011) and Voeltz *et al.* (2006) provide data suggesting that these domains adopt a hairpin conformation when inserted into the lipid bilayer. This topology results in the bulk of the hydrophobic portion of the protein being preferentially located in the outer leaflet of the lipid bilayer. The net result is that the protein has a "wedge shaped" envelope and its insertion into a lipid bilayer might create membrane curvature by providing more bulk in the outer leaflet (Collins, 2006).

1.4.3 Reticulon and DP1: protein localization and function

The first known reticulon protein, RTN1, was identified from a cDNA in neuronal tissue and subsequently characterized as an antigen specific to neuroendocrine cells. This so-called neuroendocrine-specific protein was later renamed reticulon when it was discovered to be associated with ER in COS-1 cells. Reticulons do not contain an ER localization signal *per se*, but a single RHD hydrophobic region is sufficient to target an enhanced green fluorescent protein-RTN fusion protein to the ER, whereas deletion of the RHD abolishes association with the ER (Iwahashi *et al.*, 2007). Reticulons have been shown to localize to the ER in yeast, *Arabidopsis, C elegans, Xenopus, Drosophila* and mammals. Most reticulon research has focused on RTN4 in the central nervous system and its effects on neurite outgrowth and axonal regeneration after spinal cord injury. However, the presence of reticulons in all eukaryotic organisms and their ubiquitous ER-associated expression indicate a more general role. Until now there are three areas of reticulon localization and function: ER-associated roles, oligodendrocyte-associated roles in inhibition of neurite outgrowth, and the role of reticulons in neurodegenerative diseases (Yang & Strittmatter, 2007). Concerning the ER-associated

roles, there is growing evidence that reticulons are involved in bending and shaping the ER membrane, in trafficking of material from the ER to the Golgi apparatus, and in apoptosis. A major advance in understanding of the function of reticulons came with the identification of members of the reticulon family as a key proteins involved in shaping and morphogenesis of the ER. Indeed, reticulons and DP1/REEP/Yop1 localize at the highly curved regions of the ER tubules, and in many species, their cellular depletion causes defects in the formation of the tubular ER; conversely, their overexpression leads to increased ER tubulation (Voeltz *et al.*, 2006; O'Sullivan *et al.*, 2012). In addition, *in vitro* reconstitution experiments have shown that reticulon or DP1 is sufficient to tubulate proteoliposomes (Hu *et al.*, 2008). These observations have led to a model for ER tubule formation whereby reticulons and DP1 act synergistically to trigger and stabilize membrane curvature by hydrophobic wedging (Hu *et al.*, 2011). It has been proposed that oligomerized reticulons and DP1 act as a scaffold to impose a cylindrical structure on the membrane curvature, thus generating a tubule (Hu *et al.*, 2008). By a similar mechanism, the same proteins are also involved in generating the highly curved edges of ER sheets (Shibata *et al.*, 2010).

Although reticulons are principally located within ER membranes, they have also been described at the level of Golgi and plasma membranes, suggesting that they may act also at these sites. In this context, it is interesting that several studies suggest that reticulons may be involved in the secretory pathway. For example, RTNL1 co-immunoprecipitates with a variety of SNARE proteins that are engaged in regulated secretion, and the ectopic expression of a fragment of RTNL1 in PC12 cells leads to an increased rate of growth hormone release (Steiner *et al.*, 2004).

Moreover, several lines of evidence indicate that reticulons are involved in cell death pathways, most notably in ER stress-induced apoptosis. Indeed, transient overexpression of very high levels of reticulons inducing ER stress and apoptosis, but a more moderate and sustained expression may not lead to cell death, and could in fact precondition cells against further stress (Teng & Tang, 2008).

1.4.4 Reticulon and DP1 in *Arabidopsis thaliana*

In *Arabidopsis thaliana* there are 21 genes identified as reticulons, named RTNLB (reticulon-like protein, plant subfamily B) 1-21. Although fluorescent protein fusions have not been made for all of the reticulons in plants, of those that have been made, several locate to the ER (RTNLB2, RTNLB4 and RTNLB16) but only RTNLB12 is reported to be exclusively coextensive with tubular regions of the ER (Griffing, 2010).

All RTNLBs contain a conserved RHD that comprises two large hydrophobic segments. In some cases, these segments are subdivided into smaller transmembrane domains, resulting in a number of possible transmembrane topologies, including a "W" topology in which both the N- and C-termini are located in the cytosol. Sparkes and colleagues have recently shown that five plant reticulon isoforms (RTNLB1-4 and RTNLB13) assume this "W" topology, which is probably shared by all other *Arabidopsis* RTNLB (Sparkes *et al.*, 2010).

RTNLBs show great variability in their N-terminal domains, which are involved in a wide variety of interactions. As there is virtually no functional information available about the role of reticulons in plant cells, it has been selected, for all research studies, the isoforms with the shortest N-terminal domain, RTNLB13, which comprises an intact RHD flanked by very short N- and C-terminal regions. Overexpression of RTNLB13 in tobacco leaf epidermal cells by *Agrobacterium* infiltration altered dramatically the appearance of the cortical ER: the ER tubules were no longer detectable and were replaced by clusters of large vesicle-like structures. Although, reticulon-induced ER morphology alteration has no major effect on the anterograde secretory pathway. Accordingly to the yeast and mammalian experiments, full-length TMDs are necessary for the ability of RTNLB13 to reside in the ER membrane and to form low-mobility complexes within the ER membrane (Tolley *et al.*, 2010).

In *Arabidopsis* there are 7 DP1/REEP/Yop1 homologs. The closest DP1/REEP/Yop1 homologue in plant is HVA22, one isoforms of which has been recently shown to localize to the ER, but it is not yet clear whether it can shape the ER membrane in the same way as its animal and yeast relatives. Indeed, a role for HVA22 proteins in plant ER integrity is yet to be demonstrated. However, the degree of identity with non-plant counterparts (i.e. 20-31% identity to DP1/Yop1p, which is similar to the identity between DP1 and Yop1p) suggests functional conservation (Stefano *et al.*, 2014).

1.4.5 *Drosophila* reticulon

Drosophila has a single widely expressed reticulon, reticulon 1 (Rtnl1). Rtnl1 was discovered in a screen to identify proteins enriched in axons of the developing *Drosophila* embryonic nervous system. Rtnl1 bears no closer resemblance to RTN1, RTN3 or RTN4/Nogo, but is more similar to this group than it is to RTN2.

The *Drosophila Rtnl1* locus generates several mRNA transcripts through alternative promoter usage. A total of seven transcripts are predicted for the Rtnl1 locus that encode for five different polypeptides. Each of these transcripts includes four C-terminal exons that encode the conserved RHD, again conforming to the mammalian organization.

There are experimental evidence that Rtnl1 is the only reticulon that is normally expressed by *Drosophila*. A second *Drosophila* reticulon, *Rtnl2*, is present in the *Drosophila* genome but this is possibly a retronuon with pseudogene character. *Rtnl2* has a genomic organization very distinct from other members of the reticulon family as it bears a single intron within its RHD-containing exons. Unlike *Rtnl1*, for which there are greater than 150 ESTs, there are only four ESTs identified for *Rtnl2*, all of which originate from animals that have been challenged with bacteria. Indeed there is no detectable expression of *Rtnl2* transcripts in the wild-type animal using *in situ* hybridization.

In contrast, the Rtnl1 protein is expressed ubiquitously in the embryo and shows increased expression within the nervous system at later stages of embryogenesis. The protein continues to be expressed throughout the animal in post-embryonic stages where it is retained within the nervous system with expression extending throughout axons and at presynaptic specializations. This enrichment within the nervous system is characteristic of reticulons identified in other species (Wakefield & Tear, 2006). Expression of Rtnl1 is also found in muscles and, at subcellular level, Rtnl1 localizes to ER membranes.

Recent studies have characterized a *Drosophila* model of HSP caused by loss of the human orthologue of SPG12, *Rtnl1*. The loss of Rtnl1 led to an expansion of the rough or sheet ER in larval epidermis and elevated levels of ER stress. It also caused abnormalities specifically within the distal portion of longer motor axons and in their presynaptic terminals, including disruption of the smooth ER, the microtubule cytoskeleton and mitochondria. Moreover, the loss of Rtnl1 selectively affects longer

axons, suggesting a mechanistic similarity between the cellular phenotypes of *Drosophila* Rtnl1 knockdown and spastic paraplegias that would be caused by haplo-insufficient loss-of-function or dominant negative alleles of hairpin-loop proteins.
Drosophila is the first animal model providing evidence of an ER phenotype due to the loss of Rtnl1 and shows that major arrangements of ER morphology do not noticeably affect organism survival (O'Sullivan *et al.*, 2012).

1.5 Atlastin functional partners

Human atlastins have been shown to interact physically with the ER tubule-shaping proteins reticulons and DP1. Moreover, in yeast a synergistic functional interaction has been proposed between the single atlastin homolog, the reticulon (Rtn1p and Rtn2p), and DP1 homologs (Yop1p).
Yeast cells lacking Rtn1p, Rtn2p, or both are viable, and, even in the double-deletion mutant, the morphology of the peripheral ER network appeared normal. Instead, *S. cerevisiae* lacking both reticulons and Yop1p had disrupted peripheral ER under normal growth conditions, while the nuclear envelope appeared to be unaffected. The triple-knockout mutant grew at about 2/3 the rate of wild-type cells. ER morphology defects similar to those in the triple mutant were also seen in mutants lacking Rtn1p and Yop1p. The ER appeared similar to wild-type in mutants lacking Rtn2p and Yop1p, although about 10% of the cells showed peripheral ER sheets (Voeltz *et al.*, 2006).
In yeast lacking only the atlastin homolog Sey1p, the ER resembled that in wild-type cells, comparable to observations made previously for single deletions of Rtn1p or Yop1p (Voeltz *et al.*, 2006). In cells lacking both Sey1p and Rtn1p the cortical ER was severely perturbed; most cells lacked the tubular network and instead showed aberrant structures. Similar results were obtained with cells lacking Sey1p and Yop1p. Together, these results indicate that in yeast Sey1p cooperates with Rtn1p and Yop1p to maintain the structure of the tubular ER (Hu *et al.*, 2009).

1.6 *Drosophila* as a model organism

Ever since Morgan isolated the *white* mutation in *Drosophila melanogaster* in 1910, the tiny fruit fly has made large contributions to the understanding of the genetic and molecular mechanisms of heredity and development. More recently, the remarkable

power of fruit fly genetics has been applied to study the basic mechanisms of human diseases, including those debilitating pathologies that affect the human brain.

There are several reasons why *D. melanogaster* is widely used as models of human diseases. The first and foremost reason is based on the presumption that fundamental aspects of cell biology in flies have been conserved throughout evolution in higher-order organisms such as humans (Jackson, 2008). A report demonstrating that approximately 75% of the disease-related loci in humans have at least one *Drosophila* homologue confirms the high degree of conservation present in flies. Furthermore, studies of developmental events in the fly and subsequent similar studies in higher animals have revealed a stunning degree of functional conservation of genes. These studies indicate that not only basic cell biology but also higher-order events such as organ “construction” and function are conserved.

Drosophila has an unrivalled battery of genetic tools including a rapidly expanding collection of mutants, transposon-based methods for gene manipulation and systems that allow controlled ectopic gene expression and balancer chromosomes (Cauchi & van den Heuvel, 2006). It should be possible to target endogenous wild-type copies of "disease gene" in the fly genome for inactivation (knock-out); defined mutations can also be "engineered" (knock-in) into respective endogenous genes, to create gain-of-function models (Chan & Bonini, 2000).

The above characteristics of such a minuscule system model, combined with the rapid generation time, inexpensive culture requirements, large progeny numbers produced in a single cross and a small highly annotated genome devoid of genetic redundancy, are poised to yield seminal insights into human disease (Cauchi & van den Heuvel, 2006).

For almost a century, fruit flies have been providing a useful tool to study various different subjects: form the chemical basis of mutagenesis, to the definition of genes, from developmental biology, to animal behaviour. The ability to use *Drosophila* as a powerful tool to approach pathogenetic disease mechanisms for human diseases speaks to a tremendous application in biomedical research (Chan & Bonini, 2000).

2 METHODS

2.1 Molecular biology techniques: generation of constructs

2.1.1 Cloning of Rtnl1 cDNA in pcDNA3.1/Zeo(+) plasmid

pcDNA3.1/Zeo(+) is a plasmid designed for high level expression in a variety of mammalian cell lines (see Appendix C). The Reticulon1-PB isoforms (Rtnl1) was obtained from the *Drosophila* Genomic Resource Center (LD14068). Two differently tagged Rtnl1 forms were cloned in the pcDNA3.1/Zeo(+) plasmid: HA-Rtnl1 and Myc-Rtnl1.

To insert the Myc epitope in the N-terminus of Rtnl1, cDNA was amplified from Rtnl1/BlueScript SK(-) vector using the following primers:

Forward	
Myc-Rtnl1 EcoRI	5'AGCTGAATTCATGGAACAAAAACTTATTTCTGAA GAAGATCTGTCCGCATTTGGTGAAACC3'
Reverse	
Rtnl1 XhoI	5' AGCTCTCGAGCTTTACTTGTCCTTCTCAGAC3'

To insert the HA epitope in the N-terminus of Rtnl1, cDNA was amplified using the following primers:

Forward	
HA-Rtnl1 EcoRI	5'AGCTGAATTCATGTACCCATACGATGTTCCTGAC TATGCGGGCTCCGCATTTGGTGAAACC3'
Reverse	
Rtnl1 XhoI	5' AGCTCTCGAGCTTTACTTGTCCTTCTCAGAC3'

To generate each of these constructs the protocol used was the following:

PCR reaction

Component	Volume/50 µl reaction
Rtnl1/BlueScript SK(-) template (50 µg/µl)	1 µl
5X Phusion HF buffer	10 µl
Forward (10 µM)	1 µl
Reverse (10 µM)	1 µl
10 mM dNTPs	1 µl
Phusion DNA polymerase (2U/µl)	0,5 µl
H_2O	add to 50 µl

PCR cycle

Cycle step	Temperature	Time	
Initial denaturation	98°C	30 seconds	
Denaturation	98°C	10 seconds	30 cycles
Annealing	56°C	20 seconds	
Extension	72°C	1 minute	
Final extension	72°C	10 minutes	

Restriction reactions

pcDNA3.1/Zeo(+) plasmid, HA-Rtnl1 and Myc-Rtnl1 PCR fragments were digested with restriction enzymes in the following reactions:

Component	Volume/ 50 µl reaction	Component	Volume/ 50 µl reaction
Rtnl1 PCR fragment (50ng/µl)	20 µl	pcDNA3.1/Zeo(+) plasmid (100ng/µl)	5 µl
EcoRI (10U/µl)	2 µl	EcoRI (10U/µl)	2 µl
XhoI (10U/µl)	2 µl	XhoI (10U/µl)	2 µl
10X L buffer	5 µl	10X L buffer	5 µl
H_2O	to 50 µl	H_2O	to 50 µl

Mixed products were incubated at 37°C for 1 hour and successively separated by electrophoresis through a 1% agarose gel. The bands corresponding to the Rtnl1 PCR fragments and pcDNA3.1/Zeo(+) plasmid were cut from gel and purified using the

QIAquick Gel Extraction Kit (Qiagen). Purified DNA products were eluted in 20 µl of elution buffer.

The purified DNA fragments were ligated as follows:

Ligation

Component	Volume/10 µl reaction
Purified pcDNA3.1/Zeo(+) plasmid (100ng/µl)	1 µl
Purified Rtnl1 fragment (50 ng/µl)	4 µl
10X Ligation buffer	1 µl
T4 DNA ligase (Invitrogen)	1 µl
H_2O	to 10 µl

The mixture was incubated at 22°C for 15 minutes.

Transformation

Ligation mixture was used for transformation of chemically competent DH5-alpha cells (Invitrogen). Transformed bacteria were plated on LB–ampicillin agar plates and incubated overnight at 37°C. 6 colonies for each construct were grown in LB medium with ampicillin. Plasmid DNA was successively purified by minipreparation protocol (Appendix A) and tested by restriction analysis for the right insertion.

Purification of HA-Rtnl1/pcDNA3.1/Zeo(+) and Myc-Rtnl1/pcDNA3.1/Zeo(+)

Plasmid DNA was purified from an overnight culture using a “Midi” plasmid purification kit, according to NucleoBond Xtra Midi purification protocols (Macherey-Nagel). The final pellets were re-suspended in 50 µl of TE buffer.

2.1.2 Cloning of Rtnl1 cDNA in pUAST plasmid

HA tagged version of Rtnl1 was cloned in the pUAST plasmid (Appendix C). pUAST plasmid and HA-Rtnl1/pcDNA3.1/Zeo(+) were digested with EcoRI and XhoI restriction enzymes in the following reactions:

Component	Volume/ 50 µl reaction	Component	Volume/ 50 µl reaction
HA-Rtnl1/ pcDNA3.1/Zeo(+) (50ng/µl)	20 µl	pUAST plasmid (100ng/µl)	5 µl
EcoRI (10U/µl)	2 µl	EcoRI (10U/µl)	2 µl
XhoI (10U/µl)	2 µl	XhoI (10U/µl)	2 µl
10X L buffer	5 µl	10X L buffer	5 µl
H_2O	to 50 µl	H_2O	to 50 µl

Mixed products were incubated at 37°C for 1 hour and successively separated by electrophoresis through a 1% agarose gel. The bands corresponding to the HA-Rtnl1 cDNA and pUAST plasmid were cut from gel and purified using the QIAquick Gel Extraction Kit (Qiagen). Purified DNA products were eluted in 20 µl of elution buffer.
The purified DNA fragments were ligated as follows:

Ligation

Component	Volume/10 µl reaction
Purified pUAST plasmid (100ng/µl)	1 µl
Purified HA-Rtnl1 fragment (50 ng/µl)	4 µl
10X Ligation buffer	1 µl
T4 DNA ligase (Invitrogen)	1 µl
H_2O	to 10 µl

The mixture was incubated at 22°C for 15 minutes.

Transformation

Ligation mixture was used for transformation of chemically competent DH5alpha cells (Invitrogen). Transformed bacteria were plated on LB–ampicillin agar plates and incubated overnight at 37°C. 6 colonies for each construct were grown in LB medium

with ampicillin. Plasmid DNA was successively purified by minipreparation protocol (Appendix A) and tested by restriction analysis for the right insertion.

Purification of HA-Rtnl1/pUAST

Plasmid DNA was purified from an overnight culture using a "Midi" plasmid purification kit, according to NucleoBond Xtra Midi purification protocols (Macherey-Nagel). The final pellets were re-suspended in 50 µl of TE buffer.

2.1.3 Cloning of Rtnl1 cDNA in pGEX-GST-SUMO1 plasmid

The Rtnl1 cDNA was subcloned into the pGEX-GST-SUMO1 vector (Appendix C). The cDNA was amplified from Rtnl1/BlueScript SK(-) vector using the following primers:

Forward	
Rtnl1 BamHI	5'AGCTGGATCCATGTCCGCATTTGGTGAAACC3'
Reverse	
Rtnl1 XhoI	5'AGCTCTCGAGCTTTACTTGTCCTTCTCAGAC3'

The PCR reaction is common to that used to generate tagged Rtnl1/pcDNA3.1/Zeo(+) constructs (see 2.1.1). The PCR cycle is adjusted accordingly to the annealing temperature of the primers.
PCR fragments and pGEX-GST-SUMO1 plasmid were digested with BamHI and XhoI restriction enzymes in the following reactions:

Component	Volume/ 50 µl reaction	Component	Volume/ 50 µl reaction
Rtnl1 PCR fragment (50ng/µl)	20 µl	pGEX-GST-SUMO1 plasmid (100ng/µl)	5 µl
BamHI (10U/µl)	2 µl	BamHI (10U/µl)	2 µl
XhoI (10U/µl)	2 µl	XhoI (10U/µl)	2 µl
10X L buffer	5 µl	10X L buffer	5 µl
H_2O	to 50 µl	H_2O	to 50 µl

Mixed products were incubated at 37°C for 1 hour and successively separated by electrophoresis through a 1% agarose gel. The bands corresponding to the Rtnl1 cDNA

and pGEX-GST-SUMO1 plasmid were cut from gel and purified using the QIAquick Gel Extraction Kit (Qiagen). Purified DNA products were eluted in 20 µl of elution buffer.

The purified DNA fragments were ligated as follows:

Ligation

Component	Volume/10 µl reaction
Purified pGEX-GST-SUMO1 (100ng/µl)	1 µl
Purified Rtnl1 fragment (50 ng/µl)	4 µl
10X Ligation buffer	1 µl
T4 DNA ligase (Invitrogen)	1 µl
H_2O	to 10 µl

The mixture was incubated at 22°C for 15 minutes.

Transformation and purification of Rtnl1/pGEX-GST-SUMO1

Ligation mixture was used for transformation of chemically competent DH5-alpha cells (Invitrogen). Transformed bacteria were plated on LB–ampicillin agar plates and incubated overnight at 37°C. 6 colonies for each construct were grown in LB medium with ampicillin. Plasmid DNA was successively purified by minipreparation protocol (Appendix A) and tested by restriction analysis for the right insertion.

Plasmid DNA was purified from an overnight culture using a "Midi" plasmid purification kit, according to NucleoBond Xtra Midi purification protocols (Macherey-Nagel). The final pellets were re-suspended in 50 µl of TE buffer.

2.1.4 Amplification of DP1 cDNA

The DP1 full-length complementary DNA (537 bp) was previously obtained by Reverse Transcription PCR (RT-PCR) performed on total *Drosophila* RNA. RT-PCR is a technique in which a RNA strand is "reverse" transcribed into its DNA complement, followed by amplification of the resulting DNA using a polymerase chain reaction (PCR). Transcribing a RNA strand into its DNA complement is termed reverse transcription (RT) and is accomplished through the use of a RNA-dependent DNA polymerase (reverse transcriptase). Afterwards, a second strand of DNA is synthesized through the use of a deoxyoligonucleotide primer and a DNA-dependent DNA polymerase. Subsequently, the complementary DNA and its anti-sense counterpart are amplified using traditional PCR. The original RNA template is degraded by RNase H treatment.

RT-PCR

The complementary strand from RNA template was obtained using the ThermoScript ™ RNase H^- Reverse Transcriptase (Invitrogen); for PCR reaction we used Phusion High-Fidelity DNA polymerase (Finnzymes). The entire procedure is described below.

Component	Volume/12 µl reaction
Oligo$(dT)_{20}$ (50µM)	1 µl
Total RNA	1 µg
10mM dNTP mix (10 mM each dATP, dGTP, dCTP and dTTP at neutral pH)	1 µl
H_2O	add to 12 µl

The mixture was incubated at 65°C for 5 minutes and then placed on ice. The contents of the tube was collected by brief centrifugation and to the tube were added:

Component	Volume/20 µl reaction
RT Buffer (5X)	4 µl
DTT 0.1M	1 µl
primer Oligo(dT)	1 µl
RNaseOUTTM	1 µl
Superscript III (retrotrascriptase)	200U

Contents of the tube were mixed gently and incubated at 50°C for 60 minutes. The reaction was terminated by heating at 75°C for 5 minutes. To remove the original RNA template, 1µl (2 units) of *E. coli* RNase H was added and incubated at 37°C for 20 minutes.

2.1.5 Cloning of DP1 cDNA in pcDNA3.1/Zeo(+) plasmid

The Myc tagged version of DP1 cDNA was cloned in pcDNA3.1/Zeo(+) vector (Appendix C).
To insert the Myc epitope in the N-terminus of DP1, cDNA was amplified using the following primers:

Forward	
Myc-DP1 BamHI	5'AGCTGGATCCATGGAACAAAAACTTATTTCTGAA GAAGATCTGGCCACTCAGGTGAAGCAGTTC3'
Reverse	
DP1 XhoI	5'AGCTCTCGAGCTAGTCATGCTTCAGCACTCC3'

To generate this construct the protocol used was the following:

PCR reaction

Component	Volume/50 µl reaction
DP1 cDNA template (50 µg/µl)	1 µl
5X Phusion HF buffer	10 µl
Forward (10 µM)	1 µl
Reverse (10 µM)	1 µl
10 mM dNTPs	1 µl
Phusion DNA polymerase (2U/µl)	0,5 µl
H_2O	add to 50 µl

PCR cycle

Cycle step	Temperature	Time	
Initial denaturation	98°C	30 seconds	
Denaturation	98°C	10 seconds	30 cycles
Annealing	56°C	20 seconds	
Extension	72°C	50 seconds	
Final extension	72°C	10 minutes	

Restriction reactions

pcDNA3.1/Zeo(+) plasmid and Myc-DP1 PCR fragments were digested with restriction enzymes in the following reactions:

Component	Volume/ 50 µl reaction	Component	Volume/ 50 µl reaction
Myc-DP1 PCR fragment (50ng/µl)	20 µl	pcDNA3.1/Zeo(+) plasmid (100ng/µl)	5 µl
BamHI (10U/µl)	2 µl	BamHI (10U/µl)	2 µl
XhoI (10U/µl)	2 µl	XhoI (10U/µl)	2 µl
10X L buffer	5 µl	10X L buffer	5 µl
H_2O	to 50 µl	H_2O	to 50 µl

Mixed products were incubated at 37°C for 1 hour and successively separated by electrophoresis through a 1% agarose gel. The bands corresponding to the Myc-DP1 PCR fragments and pcDNA3.1/Zeo(+) plasmid were cut from gel and purified using the QIAquick Gel Extraction Kit (Qiagen). Purified DNA products were eluted in 20 µl of elution buffer.

The purified DNA fragments were ligated as follows:

Ligation

Component	Volume/10 µl reaction
Purified pcDNA3.1/Zeo(+) plasmid (100ng/µl)	1 µl
Purified Myc-DP1 fragment (50 ng/µl)	4 µl
10X Ligation buffer	1 µl
T4 DNA ligase (Invitrogen)	1 µl
H_2O	to 10 µl

The mixture was incubated at 22°C for 15 minutes.

Transformation

Ligation mixture was used for transformation of chemically competent DH5-alpha cells (Invitrogen). Transformed bacteria were plated on LB–ampicillin agar plates and incubated overnight at 37°C. 6 colonies for each construct were grown in LB medium with ampicillin. Plasmid DNA was successively purified by minipreparation protocol (Appendix A) and tested by restriction analysis for the right insertion.

Purification of Myc-DP1/pcDNA3.1/Zeo(+)

Plasmid DNA was purified from an overnight culture using a "Midi" plasmid purification kit, according to NucleoBond Xtra Midi purification protocols (Macherey-Nagel). The final pellets were re-suspended in 50 μl of TE buffer.

2.1.6 Cloning of DP1 cDNA in pUAST plasmid

Myc tagged versions of DP1 was cloned in the pUAST plasmid (Appendix C).
To insert the Myc epitope in the N-terminus of DP1, cDNA was amplified using the following primers:

<u>Forward</u>	
Myc-DP1 NotI	5'AGCTGCGGCCGCATGGAACAAAAACTTATTTCTG AAGAAGATCTGGCCACTCAGGTGAAGCAGTTC3'
<u>Reverse</u>	
DP1 XhoI	5'AGCTCTCGAGCTAGTCATGCTTCAGCACTCC3'

The PCR reaction is common to that used to generate Myc-DP1/pcDNA3.1/Zeo(+) construct (see 2.1.5).
pUAST plasmid and Myc-DP1 fragments were digested with NotI and XhoI restriction enzymes in the following reactions:

Component	Volume/ 50 µl reaction	Component	Volume/ 50 µl reaction
Myc-Dp1/ pcDNA3.1/Zeo(+) (50ng/µl)	20 µl	pUAST plasmid (100ng/µl)	5 µl
NotI (10U/µl)	2 µl	NotI (10U/µl)	2 µl
XhoI (10U/µl)	2 µl	XhoI (10U/µl)	2 µl
10X L buffer	5 µl	10X L buffer	5 µl
H_2O	to 50 µl	H_2O	to 50 µl

Mixed products were incubated at 37°C for 1 hour and successively separated by electrophoresis through a 1% agarose gel. The bands corresponding to the Myc-DP1 cDNA and pUAST plasmid were cut from gel and purified using the QIAquick Gel Extraction Kit (Qiagen). Purified DNA products were eluted in 20 µl of elution buffer. The purified DNA fragments were ligated as follows:

Ligation

Component	Volume/10 µl reaction
Purified pUAST plasmid (100ng/µl)	1 µl
Purified Myc-DP1 fragment (50 ng/µl)	4 µl
10X Ligation buffer	1 µl
T4 DNA ligase (Invitrogen)	1 µl
H_2O	to 10 µl

The mixture was incubated at 22°C for 15 minutes.

Transformation

Ligation mixture was used for transformation of chemically competent DH5-alpha cells (Invitrogen). Transformed bacteria were plated on LB–ampicillin agar plates and incubated overnight at 37°C. 6 colonies for each construct were grown in LB medium with ampicillin. Plasmid DNA was successively purified by minipreparation protocol (Appendix A) and tested by restriction analysis for the right insertion.

Purification of Myc-DP1/pUAST

Plasmid DNA was purified from an overnight culture using a "Midi" plasmid purification kit, according to NucleoBond Xtra Midi purification protocols (Macherey-Nagel). The final pellets were re-suspended in 50 µl of TE buffer.

2.1.7 Cloning of Atlastin cDNA in pcDNA3.1/Zeo(+) plasmid

The atlastin full-length complementary DNA was previously obtained by RT-PCR performed on total *Drosophila* head RNA. The cDNA was cloned pcDNA3.1/Zeo(+) in frame with a Myc tag sequence. The atlastin/pcDNA3.1/Zeo(+)construct used for the experiments has been previously generated.

2.2 Quantitative Real-Time PCR

Real-Time Quantitative Reverse Transcription PCR (Real-Time qRT-PCR) is considered to be the most powerful, sensitive and quantitative assay for the detection of RNA levels and has become an increasingly popular technique for the analysis of gene expression. The quantification of mRNA using qRT-PCR was achieved performing a one-step reaction. With the one-step method, gene-specific primers are used and both the RT and PCR occur in one reaction tube; therefore, other genes of interest cannot be amplified for later analysis. The advantages to one-step qRT-PCR is that it is quicker to set up, less expensive to use, and involves less handling of samples, thereby reducing pipetting errors, contamination, and other sources of error.

In order to test several UAS-Rtnl1-RNAi and UAS-DP1-RNAi lines we used the SuperScript III Platinum One-Step Quantitative RT-PCR System (Invitrogen).

UAS-Rtnl1-RNAi and UAS-DP1-RNAi *Drosophila* lines were crossed with tubulin-Gal4, at 28°C; UAS-Rtnl1-RNAi/tubulin-Gal4 and UAS-DP1-RNAi/tubulin-Gal4 flies were selected and the total RNA were isolated using Trizol (Invitrogen).

We designed primers specific for Rtnl1 and for DP1; these primers anneal within the exon/exon boundary of the mRNA to allow differentiation between amplification of cDNA and potential contaminating genomic DNA:

Primers for Rtnl1 amplification:

Forward primer	5’ TTCAGAATCTACAAATCTGT 3’
Reverse primer	5’ TTTTCGTGCGACAGCGTCAG 3’

Primers for DP1 amplification:

Forward primer	5’GCGATGCTTCCAAGCCGTGGA3’
Reverse primer	5’GGTAGATGGCGCACAGACCA3’

We choose *rp49* housekeeping gene as reference gene to avoid competition between amplification of the reference gene and sample gene.

Primers for *rp49* housekeeping gene amplification:

Forward primer	5’AGGCCCAAGATCGTGAAGAA3’
Reverse primer	5’TCGATACCCTTGGGCTTGC3’

The reaction was prepared as follow:

Component single reaction	Volume/10 µl reaction
SuperScript® III RT/Platinum® *Taq* Mix (includes RNaseOUT™)	0,2 µl
2X SYBR® Green Reaction Mix	5 µl
Forward primer, 10 µM	0,2 µl
Reverse primer, 10 µM	0,2 µl
ROX Reference Dye (optional)	0,1 µl
Template (100 ng total RNA)	3 µl
DEPC-treated water	to 10 µl

The qRT-PCR was performed using standard protocols.

2.3 Biochemical techniques

2.3.1 Rtnl1 protein purification

Rtnl1 protein was expressed in bacteria and affinity purified using the following protocol.

- Rtnl1/pGEX-GST-SUMO1 was transformed into BL21(DE3) One Shot® cells using standard protocol. Transformed bacteria grew overnight at 37°C with shaking.
- 5 ml of LB containing ampicillin and chloramphenicol were inoculated with one colony of BL21(DE3) transformed with construct of interest. Grow overnight at 25°C with shaking.
- 2 L of LB containing ampicillin and chloramphenicol were inoculated with 3-4 ml of the overnight culture from the previous step, grew 2 hours at 25°C with shaking. After two hours OD_{600} should be approximately 0.4 (mid-log). When OD_{600}=0.4, IPTG was added to a final concentration of 0,1 mM to the culture. The culture was incubated at 16°C for 14-16 hours.
- The next day, recombinant fusion protein was purified, added to GST-affinity beads (Invitrogen) for one hour at 4°C and then washed (see Appendix A).
- Purified protein was eluited from the GST-affinity beads by digestion with GST-SENP2 protease overnight at 4°C.
- Purified protein was stored at -80°C for future use.

To determine the success of the expression experiment, a polyacrylamide gel was stained with Coomassie blue and looked for a band of increasing intensity in the expected size range for the recombinant protein.

2.4 Cellular biology

2.4.1 Cell culture

COS (an abbreviation for CV-1 in Origin with SV40 genes) cells are a laboratory cell line derived from monkey kidney tissue. COS cells behave like fibroblasts and were originally obtained by immortalizing CV-1 cells from the kidney of the African green monkey using a SV40 virus that produces large T antigen but does not replicate

correctly. There are several varieties of COS cell lines in common use. In this project we used COS-7 cells: COS-7 cells were developed in the 1980s using transformation with a mutant strain of SV40 coding for the wild-type T-antigen.

2.4.2 Propagation and subculturing

COS-7 cells were grown in complete DMEM medium (Lonza; see Appendix B) with 10% FBS serum and antibiotics, at 37°C in a CO_2 incubator.

Cells were passaged when growing logarithmically (at 70 to 80 % confluency) as follows:

- the cell layer was briefly washed twice with PBS to remove all traces of serum, then was added to dish the trypsin solution (see Appendix B). Cells were observed under an inverted microscope until cell layer was dispersed (usually within 5 minutes).
- Complete growth medium was added to stop trypsin action, cells were aspirated by gently pipetting and diluted into a new dish with new complete medium.

For cell count, an aliquot of the cell suspension, before plating, was mixed 1:1 with a solution of 0.1% Trypan blue (Sigma) in PBS. Trypan blue is a vital stain used to selectively colour dead cells. Hence, dead cells are shown as a distinctive blue colour under a microscope. 10 µl of the above mixture was charged on a counting chamber and viable cells in the "counting squares" were counted. The cells density was calculated as follows: average of counted cells/counting square X 10^4 X dilution factor (=2) = number of cells/ml.

2.4.3 Plasmid DNA Transfection

To introduce expression plasmids into COS-7 cells *Trans*IT-LT1® Transfection Reagent (Mirus) was used. Transfection Reagent is a mix of cationic lipids. The basic structure of cationic lipids consists of a positively charged head group and one or two hydrocarbon chains. The charged head group governs the interaction between the lipid and the phosphate backbone of the nucleic acid and facilitates DNA condensation. The positive surface charge of the liposomes also mediates the interaction of the nucleic acid and the cell membrane allowing for fusion of the liposome/nucleic acid ("transfection complex") with the negatively charged cell membrane. The transfection complex is thought to enter the cell through endocytosis. Once inside the cell, the complex must

escape the endosomal pathway, diffuse through the cytoplasm and enter the nucleus for gene expression.

Protocol

In a twelve-well, one day before transfection, 1 x 10^5 cells were plated in 1,5 ml of DMEM medium without antibiotics so that cells were 90-95% confluent at the time of transfection.

For each transfection sample, the complexes were prepared as follows:

- ✓ DNA (1,5 µg) was diluted in 200 µl of Opti-MEMI Reduced-Serum Medium (Gibco) and mixed gently.
- ✓ *Trans*IT-LT1 was mixed gently before use, then 3 µl of it were added to diluted DNA mixture, mixed gently and incubated for 20 minutes at room temperature.

The 200 µl of complexes were added to each well containing cells and medium.

Cells were incubated at 37°C in a CO_2 incubator for 24 hours prior to testing for transgene expression.

2.4.4 Immunocytochemistry (ICC)

For immunocytochemistry, the day before transfection cells were plated on a glass coverslip previously sterilized.

The procedure used is divided into the below steps:

- ✓ **Fixation**: one day after transfection, the cells were fixed in 4% paraformaldehyde in PBS pH 7.4 for 10 minutes at room temperature. The cells were then washed tree times with PBS to eliminate paraformaldehyde.
- ✓ **Permeabilization**: To permeabilize cell membranes and improving the penetration of the antibody, the cells were incubated for 10 minutes with PBS containing 0.1% Triton X-100 (Applichem).
- ✓ **Blocking and incubation**: Cells were incubated with 10% serum in PBS for 10 minutes to block non specific binding of the antibodies. Primary antibodies, diluted in PBS with 5% serum, were applied for 1 hour in a humidified chamber at 37°C. Cells were washed three times with PBS and then secondary antibodies, diluted in PBS, were applied for 1 hour in a humidified chamber at 37°C.
- ✓ **Mounting and analysis**: Coverslips were mounted with a drop of the mounting medium Mowiol (Sigma). Images were collected with a Nikon C1 confocal

microscope and analysed using either Nikon EZ-C1 (version 2.1) or NIH ImageJ (version 1.32J) softwares.

The following antibodies were used: mouse anti-Myc (1:1000, Sigma), rabbit anti-HA (1:500, Santa Cruz Biotechnology), rabbit anti-calnexin (1:200, Santa Cruz Biotechnology).

Secondary antibodies for immunofluorescence (Cy5 and Cy3 conjugates from Jackson Laboratories and Alexa Fluor 488 conjugates from Invitrogen) were used at 1:1000.

2.5 Microscopy

2.5.1 Immunohistochemistry

Immunostaining was performed on wandering third instar larvae raised at 28°C. After harvesting larvae, they were dissected dorsally in phosphate-buffered saline (PBS) and fixed in 4% paraformaldeyde for 15 minutes. Preparations were then washed in PBS. Coverslips were mounted with a drop of the mounting medium Mowiol (Sigma).

2.5.2 Fluorescence loss in photobleaching (FLIP)

Experimental larvae expression UAS-GFP-KDEL were dissected in Ca^{2+}-free HL3 and analysed using a Nikon C1 confocal microscope with a 60X water immersion objective.
Two different ROI for each genotype distributed along muscle 6 or 7 in the abdominal segment 3 or 4 were selected and bleached by 20 iterations, at 100% laser power, followed by three scanning images every 15 seconds. The bleached protocols were repeated for 45 minutes.
To create fluorescence recovery curves, fluorescence intensities were transformed into a 0-100% scale and were plotted using Excel software.
Each FLIP experiment was repeated at least three times.

2.5.3 Image analysis

Confocal images were acquired through x40 or x60 CFI Plan Apochromat Nikon objectives with a Nikon C1 confocal microscope and analyzed using either Nikon EZ-C1 or NIH ImageJ softwares.
In the quantification experiments, seven independent transfection experiments were performed and approximately 100 cells were scored in each experiment.
P values reported in this study are two tailed values and derived from a Student's t-test, assuming unequal variances. Standard errors are reported as S.E.M.

2.5.4 Electron microscopy

Drosophila third instar larva brains were fixed in 4% paraformaldehyde and 2% glutaraldehyde and embedded as described earlier. EM images were acquired from thin

sections under a FEI Tecnai-12 electron microscope. EM images of individual neurons for the measurement of the length of ER profiles were collected from three brains for each genotype. At least 20 neurons were analyzed for each genotype. Quantitative analyses were performed with ImageJ software.

2.6 *Drosophila* transformation

2.6.1 *Drosophila melanogaster* life cycle

Fruit flies begin their lives as an embryo in an egg. This stage lasts for about one day when the embryo develops into a larva. The larval development, comprising three different stages, lasts about six days, then the larva stops moving and forms a pupa. *Drosophila* stays in the pupa for about five days. During this time, the metamorphosis, or change, from larva to adult occurs. When the adults emerge from the pupa they are fully formed. They become fertile after about ten hours, copulate, the females lay eggs, and the cycle begins again. The whole life cycle takes about 12-14 days (Fig. 4).

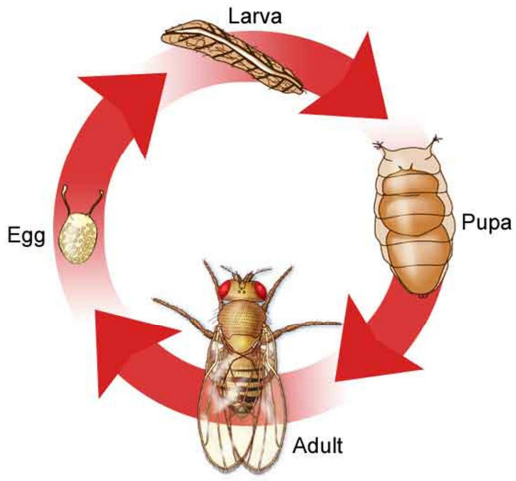

Fig. 4 – *Drosophila melanogaster* life cycle.

2.6.2 Microinjection

The HA-Rtnl1/pUAST and Myc-DP1/pUAST were prepared and sent to BestGene Inc. for *Drosophila* embryo injection. A white mutant strain, w^{1118}, was used for microinjection. These flies have white eyes allowing the detection of the transgene insertion in the offspring.

2.6.3 Characterization of transgenic lines

Hatching adults (F0) were separated by sex. Each male was crossed to two virgin w^{1118} female and each female to two or more w^{1118} males. Crosses were performed in separate vials of standard food. The F1 offspring was screened for transformant individuals where exogenous DNA was inserted in the fly genome. Transgenic flies selected for the red eye phenotype will be crossed with "balancer" lines that carry dominant phenotypic markers to generate a stable transgenic line avoiding loss of the transgene.

F1 individuals may bear one transgene insertion on any of the chromosomes: X, II, III or IV. Transgenes inserted on the fourth chromosome are very rare as this chromosome is rather small and essentially heterochromatic. If the insertion lays on the second chromosome each transgenic F1 fly is crossed with the second chromosome balancer stock Sm6a/TfT, carrying the dominant morphological marker *CyO* that produces curly wings. Individuals of the F2 carrying the transgene and the *CyO* marker were crossed to generate a stable transgenic line (Fig. 5). If in the F2 progeny there are individuals with white eyes the insertion is localized on another chromosome.

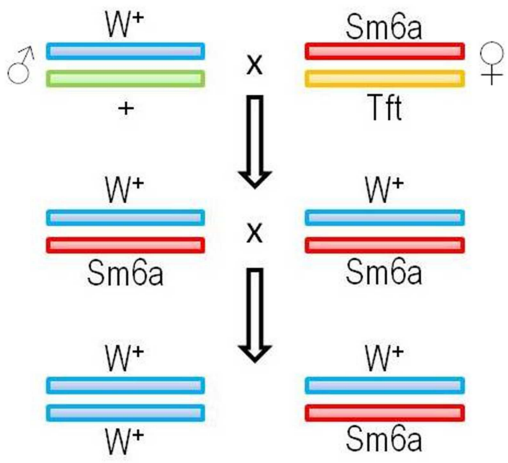

Fig. 5 – Cross with II chromosome balancer.

If the insertion lays on the third chromosome each transgenic F1 fly is crossed with the third chromosome balancer stock TM3/TM6, carrying the dominant morphological marker *Sb* that produces stubble hairs. Individuals of the F2 carrying the transgene and the *Sb* marker were crossed to generate a stable transgenic line (Fig. 6).

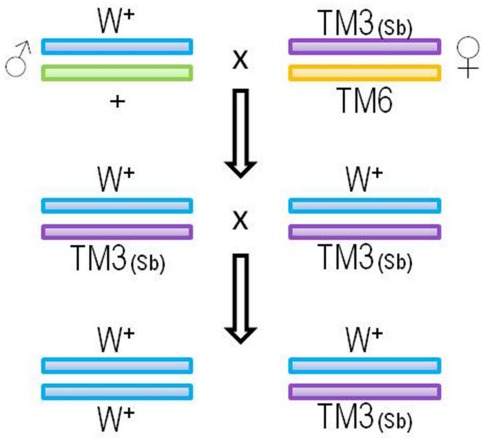

Fig. 6 – Cross with III chromosome balancer.

If the insertion lays on the X chromosome each transgenic F1 male fly is crossed with the X chromosome balancer stock Fm7/Sno, carrying the dominant morphological marker *Bar* that produces heart-shaped eyes. If the insertion is occurred in the X chromosome, all the F1 females have heart-shaped red eyes. These female were crossed with males of the X chromosome balancer stock Fm7/Y to generate a stable transgenic line (Fig. 7).

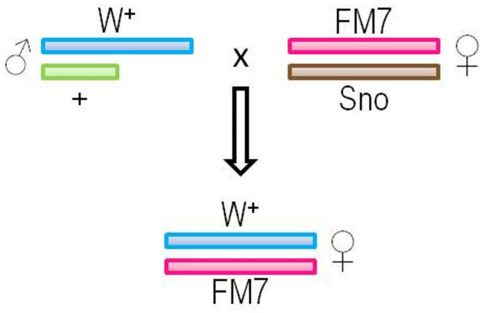

Fig. 7 – Cross with X chromosome balancer.

2.6.4 *Drosophila* genetics

Fly culture and transgenesis were performed using standard procedures. Several transgenic lines for UAS-HA-Rtnl1 and UAS-Myc-DP1 were generated and tested.

Drosophila strains used: GMR-Gal4; tubulin-Gal4; armadillo-Gal4; tubulin-Gal4,UAS-GFP-KDEL; GMR-Gal4, UAS-atlastin/+. $Rtnl1^{1}$ and atl^{2} mutant lines were previously described (Wakefield S. & Tear G., 2006; Lee M. *et al.*, 2009).

UAS-Rtnl1-RNAi lines were obtained from Vienna *Drosophila* RNAi Center (GD-7866, GD-33919; KK-110545).
UAS-DP1-RNAi line was obtained from Vienna *Drosophila* RNAi Center (KK-105290).

Control genotypes varied depending on individual experiments, but always included promoter-Gal4/+ and UAS-transgene/+ individuals.

Lifespan experiments were performed with 200 animals for each genotype. Flies were collected 1 day after eclosion and placed in vials containing 50 animals. The animals were maintained at 25°C, transferred to fresh medium every day, and the number of dead flies was counted. Lifespan experiments were repeated at least 3 times.

APPENDIX A: General protocols

Transformation of chemiocompetent cells

- Gently thaw the chemiocompetent cells on ice.
- Add ligation mixture to 50 µl of competent cells and mix gently.
- Incubate on ice for 30 minutes.
- Heat-shock the cells for 30 seconds at 42°C without shaking.
- Immediately transfer the tube to ice.
- Add 450 µl of room temperature SOC medium.
- Shake horizontally at 37°C for 1 hour.
- Spread 20 µl and 100 µl from the transformation on pre-warmed selective plates and incubate overnight at 37°C.

Preparation of plasmid DNA by alkaline lysis with SDS: minipreparation

Plasmid DNA may be isolated from small-scale (1-3 ml) bacterial cultures by treatment with alkali and SDS.

- Inoculate 3 ml of LB medium (Appendix B) containing the appropriate antibiotic with a single colony of transformed bacteria. Incubate the culture overnight at 37°C with vigorous shaking.
- Pour 1.5 ml of the culture into a microfuge tube. Centrifuge at maximum speed for 30 seconds in a microfuge. Store the unused portion of the original culture at 4°C.
- When centrifugation is complete, remove the medium by aspiration, leaving the bacterial pellet as dry as possible.
- Resuspend the bacterial in 100 µl of ice-cold Alkaline lysis solution I (Appendix B) by vigorous vortexing.
- Add 200 µl of freashly prepared Alkaline lysis solution II (Appendix B) to each bacterial suspension. Close the tube tightly, and mix the contents by inverting the tube rapidly five time. Do not vortex. Store the tube on ice.
- Add 150 µl of ice-cold Alkaline lysis solution III (Appendix B). Close the tube and disperse Alkaline lysis solution III through the viscous bacterial lysate by inverting the tube several times. Store the tube on ice 3-5 minutes.

- Centrifuge the bacterial lysate at maximum speed for 5 minutes at 4°C in a microfuge. Transfer the supernatant to a fresh tube.
- Precipitate nucleic acids from the supernatant by adding 2 volumes of ethanol at room temperature. Mix the solution by vortexing and then allow the mixture to stand 2 minutes at room temperature.
- Collect the precipitate of nucleic acid by centrifugation at maximum speed for 10 minutes at 4°C in a microfuge.
- Remove the supernatant by gentle aspiration. Stand the tube in an inverted position on a paper towel to allow all of the fluid to drain away. Use a pipette tip to remove any drops of fluid adhering to the walls of the tube
- Add 2 volumes of 70% ethanol to the pellet and invert the closed tube several times. Recover the DNA by centrifugation at maximum speed for 5 minutes at 4°C in a microfuge.
- Again remove all the supernatant by gentle aspiration.
- Dissolve the nucleic acids in 50 µl of TE buffer (pH 8.0) or distillated autoclavated water containing 20 µg/ml DNase-free RNase A (pancreatic RNase). Vortex the solution gently for a few seconds. Store the DNA solution at -20°C.

Purification of recombinant fusion protein

- 14-16 hours after induction with IPTG, centrifuge the 2 L of the culture at 4000 rpm for 15 minutes at 4°C.
- When centrifugation is completed, remove the medium by aspiration, leaving the bacterial pellet as dry as possible.
- Resuspend the bacterial in 50 ml of buffer A200 (Appendix B) by vigorous vortexing.
- Centrifuge at 4000 rpm for 10 minutes at 4°C.
- When centrifugation is completed, remove the medium by aspiration and add 40 ml of Breaking buffer.
- Sonicate the solution for 20 seconds for 6 times.
- Centrifuge at 6000g for 30 minutes at 4°C. In the meanwhile, centrifuge GST-affinity beads at 700g for 5 minutes at 4°C and then wash the beads with 20 ml of Buffer Wash1 (Appendix B).

- When the centrifugation is completed, add the supernatant to the GST-affinity beads and incubate for 1 hour at 4°C.
- After the incubation, centrifuge GST-affinity beads at 700g for 5 minutes at 4°C.
- Again remove all the supernatant by gentle aspiration and wash the resin with 20 ml of Buffer Wash 1 for two times.
- Wash the resin with 10 ml of Buffer Wash 2 (Appendix B) for 5 times.
- Add 700 µl of Buffer W2 (Appendix B) and GST-SENP2 protease and incubate the solution overnight at 4°C.
- The next day, centrifuge GST-affinity beads at 700g for 30 seconds at 4°C and collected the supernatant containing the purified protein.
- Store the purified protein at -80°C.

APPENDIX B: Stocks and solutions

LB Medium (Luria-Bertani Medium)

Bacto-tryptone	10g
Yeast extract	5g
NaCl	10g
H_2O	to 1 Liter

Autoclave.

LB Agar

Bacto-tryptone	10g
Yeast extract	5g
NaCl	10g
Agar	20g
H_2O	to 1 Liter

Adjust pH to 7.0 with 5N NaOH. Autoclave.

LB–Ampicillin Agar

Cool 1 Liter of autoclaved LB agar to 55° and then add 100 ug/ml filter-sterilized ampicillin. Pour into petri dishes (~30 ml/100 mm plate).

SOC medium

Bacto-tryptone	20g
Yeast extract	5g
NaCl	0,5g
KCl 1M	2,5 ml
H_2O	to 1 Liter

Adjust pH to 7.0 with 10N NaOH, autoclave to sterilize and add 20 ml of sterile 1M glucose immediately before use.

Alkaline lysis solution I

Glucose 50 mM

Tris HCl 25 mM (pH 8.0)

EDTA 10 mM (pH 8.0)

Solution I can be prepared in batches of approximately 100 ml, autoclaved for 15 minutes and stored at 4 °C.

Alkaline lysis solution II

NaOH 0.2N

SDS 1%

Alkaline lysis solution III

Potassium acetate 3M

Glacial acetic acid 11.5% (v/v)

TE Buffer

Tris-HCl 10 mM (pH 7.5)

EDTA 1 mM

Buffer A200

Hepes 25 mM

KCl 200 mM

Breaking Buffer

HEPES 25 mM

KCl 200 mM

Glycerol 10%

β-mercaptoethanol 2 mM

EDTA 2 mM

Triton X-100 4%

1 tablet of complete protease inhibitor tabs EDTA-free

Buffer Wash 1

HEPES 25 mM

KCl 400 mM

Glycerol 10%

β-mercaptoethanol 2 mM

EDTA 1mM

Triton X-100 1%

Buffer Wash 2

HEPES 25 mM

KCl 100 mM

Glycerol 10%

EDTA 1mM

Triton X-100 0,1%

Buffer W2

HEPES 25 mM

KCl 100 mM

EDTA 1mM

Triton X-100 0,1%

Phoshate Buffered Saline (PBS)

KH_2PO^4	15 g/L
NaCl	9 g/L
Na_2HPO^4	8 g/L

***Drosophila*'s food**

Agar	15 g
Yeast extract	46,3 g
Sucrose	46,3 g
H_2O	to 1Liter

Autoclave and then add 2 g of Nipagine dissolved in 90% ethanol.

APPENDIX C: Plasmids

pcDNA3.1/Zeo(+) (Invitrogen)

pcDNA3.1/Zeo (+) is an expression vector, derived from pcDNA3.1, designed for high-level stable and transient expression in a variety of mammalian cell lines. To this aim, it contains Cytomegalovirus (CMV) enhancer-promoter for high-level expression; large multiple cloning site; Bovine Growth Hormone (BGH) polyadenylation signal; transcription termination sequence for enhanced mRNA stability and Zeocin resistance coding region.

pUAST vector

pUAST is a P-element based vector for transgenesis in *Drosophila*. pUAST consists of five tandemly arrayed optimized Gal4 binding sites followed by the hsp70 TATA box and transcriptional start, a polylinker containing unique restriction sites and the SV40 small T intron and polyadenylation site. These features are included in a P-element vector (pCaSpeR3) containing the P-element ends (P3' and P5') and the white gene which acts as a marker for successful incorporation into the *Drosophila* genome.

pGEX-GST vector

The pGEX plasmids are designed for inducible, high level intracellular expression of genes or gene fragments as fusions with *Schistosoma japonicum* GST. The GST gene fusion vectors contain a *tac* promoter for chemically inducible, high-level expression, an internal *lacI*^{q} gene for use in any *E. coli* host, very mild elution conditions for release of fusion proteins from the affinity matrix, thus minimizing effects on antigenicity and functional activity and a PreScission, thrombin or factor Xa protease recognition sites for cleaving the desired protein from the fusion product.

3 RESULTS

3.1 Reticulon

3.1.1 Rtnl1 and atlastin display an antagonistic genetic interaction

The *Drosophila* genome contains one functional reticulon protein, Rtnl1. *Rtnl1* encodes several differentially expressed isoforms that vary in the length of the N-terminal region but share a highly conserved RHD domain responsible for membrane insertion (Wakefield & Tear, 2006). The mammalian atlastin GTPases have been proposed to interact with the reticulons and a synergistic genetic interaction between the functional ortholog of the atlastin Sey1p and reticulon has been reported in yeast (Hu *et al.*, 2009).

We used *Drosophila* to investigate the functional relationship between atlastin and reticulon in higher eukaryotes. To address the function of reticulon in the shaping of endoplasmic reticulum membranes in a multicellular organism *in vivo*, we investigated whether the single functional *Drosophila* reticulon gene, Rtnl1, interacts with the single ER membrane fusion protein atlastin in flies.

Null mutant lines for both reticulon and atlastin, called $Rtnl^1$ and atl^2, are available. Lee *et al.* have generated deletion mutants by imprecise excision of atl^1, a viable P-element insertion in the first intron of the *Drosophila* atlastin gene. Among the mutants, atl^2 had an approximately 1.6 kb deletion within the atlastin locus that removed the DNA encoding exon 3 through exon 4. The atlastin gene is essential, since mutants bearing the atl^2 allele in homozygosis survive only to pupal stages with few adult escapers. The escapers have smaller body size compared to w^{1118} wild-type control flies and are both female and male sterile (Lee *et al.*, 2009).

A *Drosophila* Rtnl1 loss-of-function line (referred to as $Rtnl1^1$) is also available. To generate a mutation that removed all reticulon function, a targeted gene deletion strategy was employed to delete the RHD, a domain common among all Rtnl isoforms. $Rtnl1^1$ homozygous flies are viable, fertile and exhibit no obvious developmental abnormalities (Wakefield & Tear, 2006).

In order to investigate the presence of a potential genetic interaction between atlastin and reticulon, we performed a series of genetic crosses to generate double mutant flies that simultaneously lack both genes ($Rtnl1^1/Rtnl1^1;atl^2/atl^2$). We first analyzed flies lacking atlastin or reticulon separately. In agreement with the data reported by Lee *et al.*

and Wakefield & Tear, we found that homozygous atl^2 individuals die at the pupa stage with a 2% rate of escapers and that homozygous $Rtnl^1$ flies are viable and normal. Surprisingly, we found that combining the two mutations in homozygosity resulted in 84% adult survival (Fig.8A), demonstrating that loss of $Rtnl^1$ has the ability to rescue the lethality associated with depletion of atlastin. Thus, this result indicates that a strong antagonistic genetic interaction between atlastin and reticulon exists in *Drosophila*. Although viable, the fertility and the body size of $Rtnl1^1/Rtnl1^1;atl^2/atl^2$ flies are not rescued: indeed double mutant flies are sterile and have a small body size. Moreover, the lifespan of double mutant flies is half that of the double heterozygotes $Rtnl1^1/+;atl^2/+$ (Fig. 8B) indicating that animals lacking both genes predictably do not fare well.

We confirmed the antagonistic interaction between reticulon and atlastin also in the *Drosophila* eye. To do this, we used UAS-Rtnl1-RNAi transgenic flies, whose expression can be controlled spatially and temporally using the Gal4/UAS expression system (Brand & Perrimon, 1993). In the UAS-Rtnl1-RNAi fly line, the transgene is placed downstream of a UAS (Upstream Activating Sequence) transcriptional enhancer, that consists of Gal4-binding sites. The transgene is activated when these flies are crossed to transgenic flies that express Gal4, also known as “drivers”. The Gal4 gene is placed downstream of a cell- or tissue- specific promoter, allowing the expression of the transgenic protein only in a specific cell or tissue type, in the progeny. A wide array of cell type and developmentally regulated Gal4 “driver” lines have been made and characterized. Examples include the pan-neuronal promoter elav (embryonic lethal abnormal vision) or the eye specific promoter GMR (Glass Multimer Response).

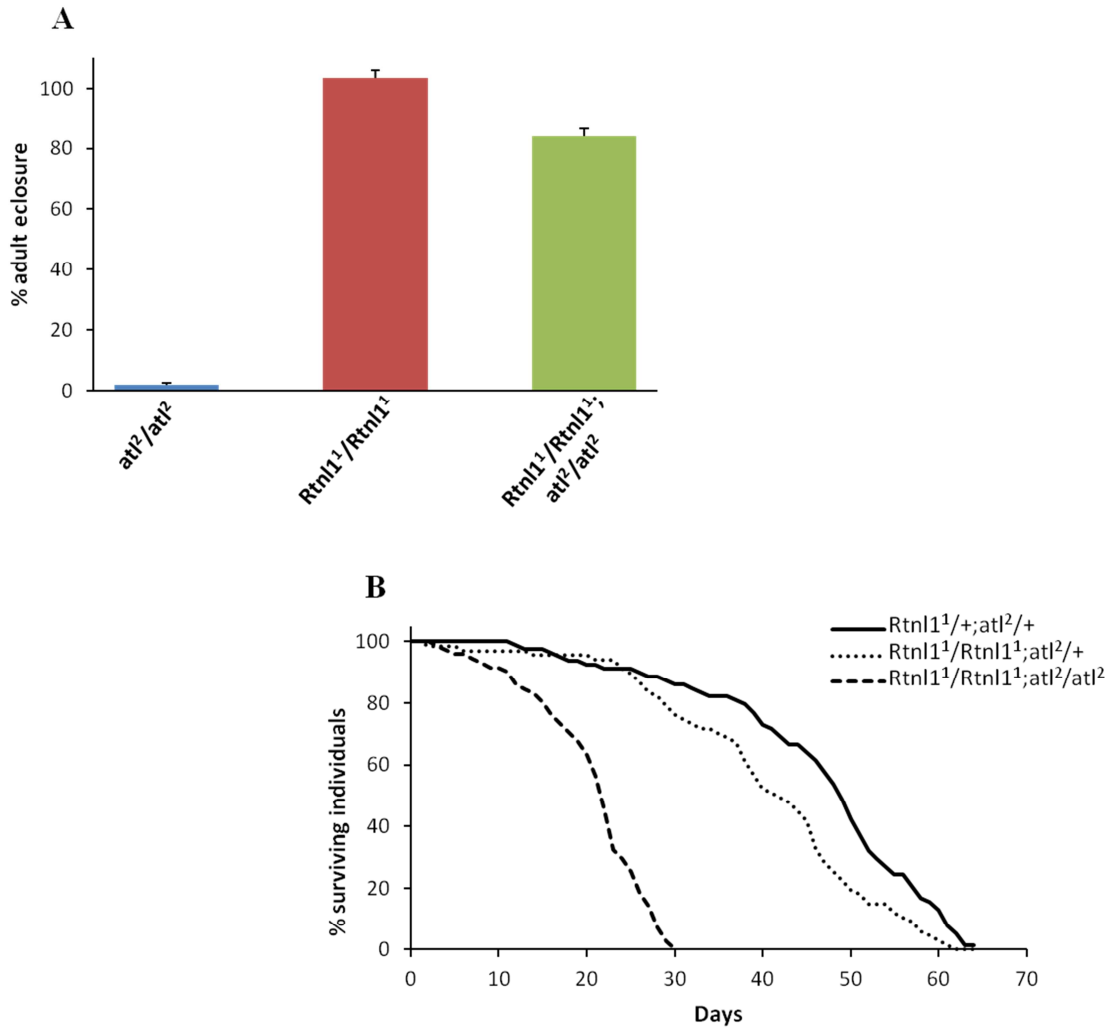

Fig. 8 – Loss of Rtnl1 suppresses the lethality caused by loss of atlastin. (**A**) The histogram displays the percentage of surviving adults, expressed as the ratio of observed over expected individuals, for the indicated genotypes. (**B**) Longevity curve showing that $Rtnl1^{1}/Rtnl1^{1};atl^{2}/atl^{2}$ double mutant flies have shortened lifespan.

UAS-Rtnl1-RNAi fly lines are available at the Vienna *Drosophila* RNAi Center (GD-7866; GD-33919; KK-110545). To validate the efficiency and the specificity of these RNAi lines, we induced ubiquitous expression of UAS-Rtnl1-RNAi using the driver tubulin-Gal4 and tested if the transcriptional levels of the Rtnl1 mRNA were reduced compared to wild type w^{1118} control flies using quantitative Real Time PCR (qRT-PCR). Based on the sequence of Rtnl1, we designed a couple of primers to amplify a region spanning from exon 5 to exon 6; the presence of an intron between the exons allows to differentiate between amplification of the cDNA and potentially contaminating genomic DNA. The amplicon size was about 100 bp. In order to maximize the effect of *in vivo* transgenic RNAi, we maintained the cross at 28°C, since Gal4 activity is temperature dependent. UAS-Rtnl1-RNAi/tubulin-Gal4 flies were

selected to isolate total mRNA and qRT-PCR was performed. The level of Rtnl1 mRNA was normalized to the mRNA level of the housekeeping *rp49* gene. We found that all three UAS-Rtnl1-RNAi lines substantially reduced Rtnl1 mRNA, demonstrating that they are efficacious in abating Rtnl1 function. In particular, UAS-Rtnl1-RNAi GD-7866 reduced the endogenous levels of Rtnl1 mRNA by 98%, UAS-Rtnl1-RNAi GD-33919 by 88%, and UAS-Rtnl1-RNAi KK-110545 by 92% (Fig. 9). As expected based on the absence of gross defects in null mutant flies, UAS-Rtnl1-RNAi/tubulin-Gal4 individuals are viable and do not display phenotypic abnormalities.

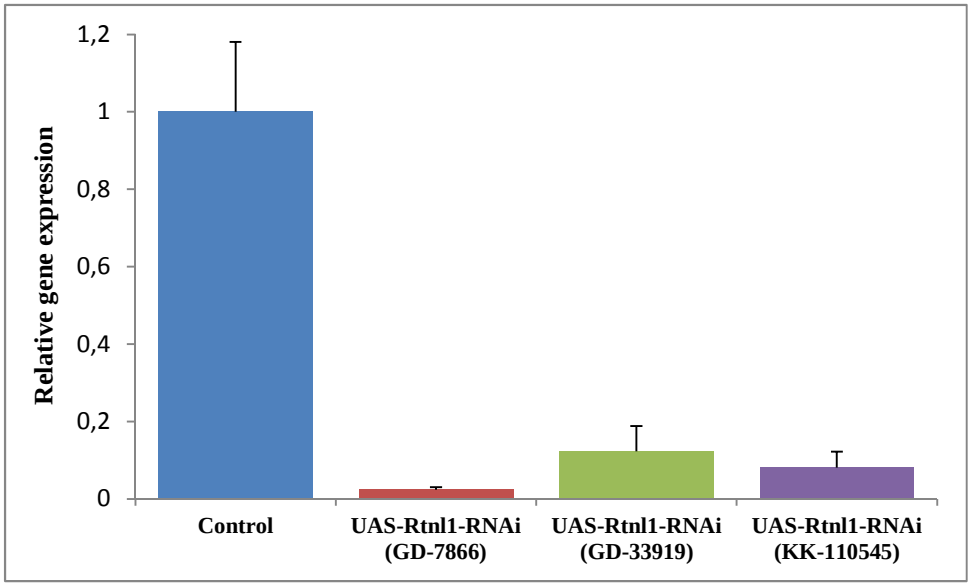

Fig. 9 – Bar graph illustrating real time PCR data demonstrating a reduction of Rtnl1 mRNA in UAS-Rtnl1-RNAi flies compared to the host gene *rp49*. Assays were performed in triplicate and results shown are representative of two independent experiments.

To examine the interaction between reticulon and atlastin in the *Drosophila* eye, we crossed UAS-Rtnl1-RNAi flies with flies overexpressing atlastin under the control of the eye specific driver GMR-Gal4 (GMR-Gal4,UAS-atlastin/+). It has been already demonstrated that ectopic expression of atlastin in the developing eye causes a small and rough eye phenotype (Fig. 10c; Orso *et al.*, 2009). In contrast, loss of Rtnl1, mediated by RNAi does not perturb eye morphology (Fig. 10b). As expected if atlastin and reticulon function antagonistically, RNAi-mediated loss of reticulon in an eye simultaneously expressing atlastin resulted in an enhancement of the atlastin-dependent small eye phenotype (Fig. 10d). Taken together the results of our genetic analyses strongly suggest that atlastin and reticulon display a robust antagonistic functional interaction in *Drosophila*.

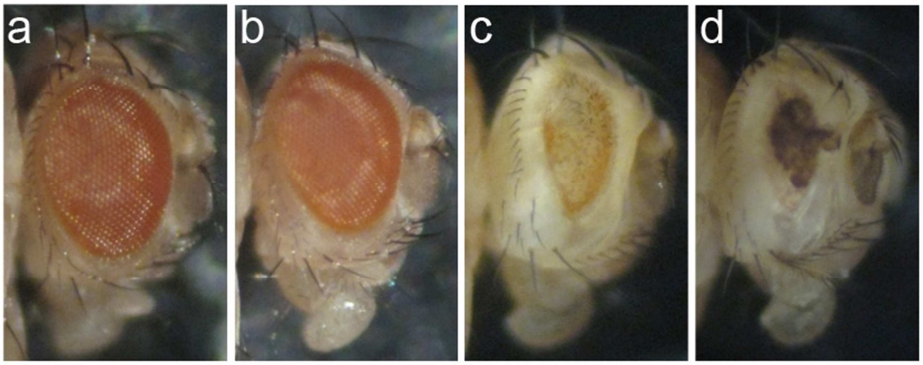

Fig. 10 – Reticulon and atlastin show opposing activities. (**a**) Adult *Drosophila* control eye (GMR-Gal4/+). (**b**) Loss of Rtnl1 using GMR-Gal4 does not perturb the eye phenotype (GMR-Gal4/+;UAS-Rtnl1-RNAi/+). (**c**) Overexpression of atlastin using GMR-Gal4 causes a small eye (GMR-Gal4,UAS-atlastin/+). (**d**) Loss of Rtnl1 enhances the GMR-atlastin small eye phenotype (GMR-Gal4,UAS-atlastin/+; UAS-Rtnl1-RNAi/+).

3.1.2 Loss of Rtnl1 causes elongation of ER profiles

The reticulon family of proteins has been implicated in determining the shape of the tubular ER (Hu *et al.*, 2008; Hu *et al.*, 2009), thus, we reasoned that the simplest explanation underlying the interaction between Rtnl1 and atlastin would depend on the membrane remodeling activity of Rtnl1.

We performed immunofluorescence experiments on larva muscles lacking Rtnl1 in order to examine ER integrity *in vivo* using the ER/Sarcoplasmic reticulum (SR) luminal marker GFP-KDEL. We did not observe any apparent discrepancies in the distribution, intensity or localization of the ER/SR marker between $Rtnl1^{1}$ and control

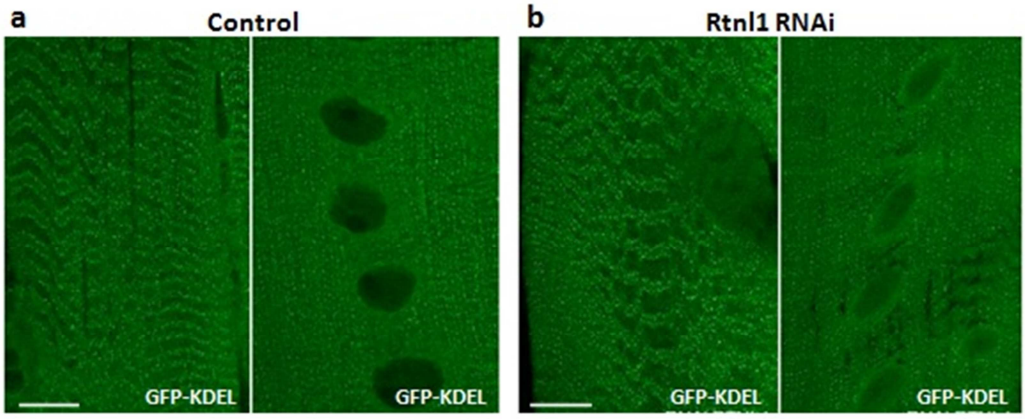

Fig. 11 – Immunofluorescence analysis of tissues depleted of Rtnl1 does not show morphological defects of the ER/SR. (**a**) Control w^{1118} and (**b**) tubulin-Gal4,UAS-GFP-KDEL/UAS-Rtnl1-RNAi body wall muscles of third instar larva were analyzed by fluorescence confocal microscopy. Scale bar: 10 µm.

Drosophila muscles (Fig. 11).

Therefore, to assess ER morphology in greater detail, we resorted to electron microscopy (EM) to visualize the neuronal ER in third instar larva brains. The length of each ER profile imaged was measured. Data analysis showed that in control neurons ER profile length was consistent (average length 862±58 nm) with that previously reported (Orso *et al.*, 2009) while $Rtnl1^1$ neurons displayed very elongated ER profiles (average length 1981±178 nm; Fig. 12A and D). Size distribution revealed that the most abundant class of ER profiles in $Rtnl1^1$ neurons was the longest (>2500 nm). This class was virtually absent in control neurons where the most represented class was instead that between 500-1000 nm (Fig. 12E). Furthermore, EM tomography showed that these long profiles found in $Rtnl1^1$ neurons correspond to elongated and unbranched ER sheets (Fig. 12B), in agreement with previous reports (Anderson & Hetzer, 2008; O'Sullivan *et al.*, 2012). To demonstrate that the observed increase in length of ER profiles was due to loss of Rtnl1, we performed rescue experiments by expressing wild-type Rtnl1 in $Rtnl1^1$ null mutant background. We generated UAS-Rtnl1 transgenic lines by cloning the Rtnl1 cDNA in frame with an N-terminal HA tag in the pUAST vector designed for P-element mediated insertion in the *Drosophila* genome. This construct was microinjected in *Drosophila* embryos and the transgenic lines obtained were mapped to a specific chromosome and balanced. UAS-HA-Rtnl1 was ubiquitously expressed with the armadillo-Gal4 promoter in the $Rtnl1^1$ background through a series of genetic crosses. The presence of Rtnl1 fully rescued the phenotype, indicating that loss of Rtnl1 is the cause of ER profile elongation (Fig. 12C and D).

We then used EM to examine the antagonistic relationship between reticulon and atlastin at the ultrastructural level. It has been previously demonstrated that loss of atlastin causes ER fragmentation (Orso *et al.*, 2009). Analysis of atl^2 larva neurons confirmed that the average length of ER profiles was much shorter (303±40 nm) than in controls (862±58 nm; Fig. 12A and D). Moreover, EM tomography-based 3D reconstruction of atl^2 mutant ER revealed a disconnected network composed of separated elements (Fig. 12B). We analyzed ER morphology in $Rtnl1^1/Rtnl1^1;atl^2/atl^2$ double mutant brains and we found that the observed rescue of viability was accompanied by a robust rescue of ER length. Double mutant profiles had an average length (1081±99 nm) comparable to that of control profiles and overlapping size distribution (Fig. 12A and D). 3D reconstruction showed that the ER network in $Rtnl1^1/Rtnl1^1;atl^2/atl^2$ neurons is very similar to that of controls, comprising

interconnected tubular and sheet-like elements (Fig. 12B). Thus, under physiological conditions, Rtnl1 could oppose the fusogenic activity of atlastin, perhaps mediating ER membrane scission, a process whose inactivation would result in the presence of longer ER profiles. The greatly diminished amount of long sheets in $Rtnl1^{1}$ mutants upon atlastin removal indicates that atlastin-mediated fusion contributes substantially to the formation of these structures. Moreover, the normal appearance of the ER network in $Rtnl1^{1}/Rtnl1^{1};atl^{2}/atl^{2}$ double mutants suggests that Rtnl1 is not absolutely required to maintain the tubular ER network (Fig. 12B).

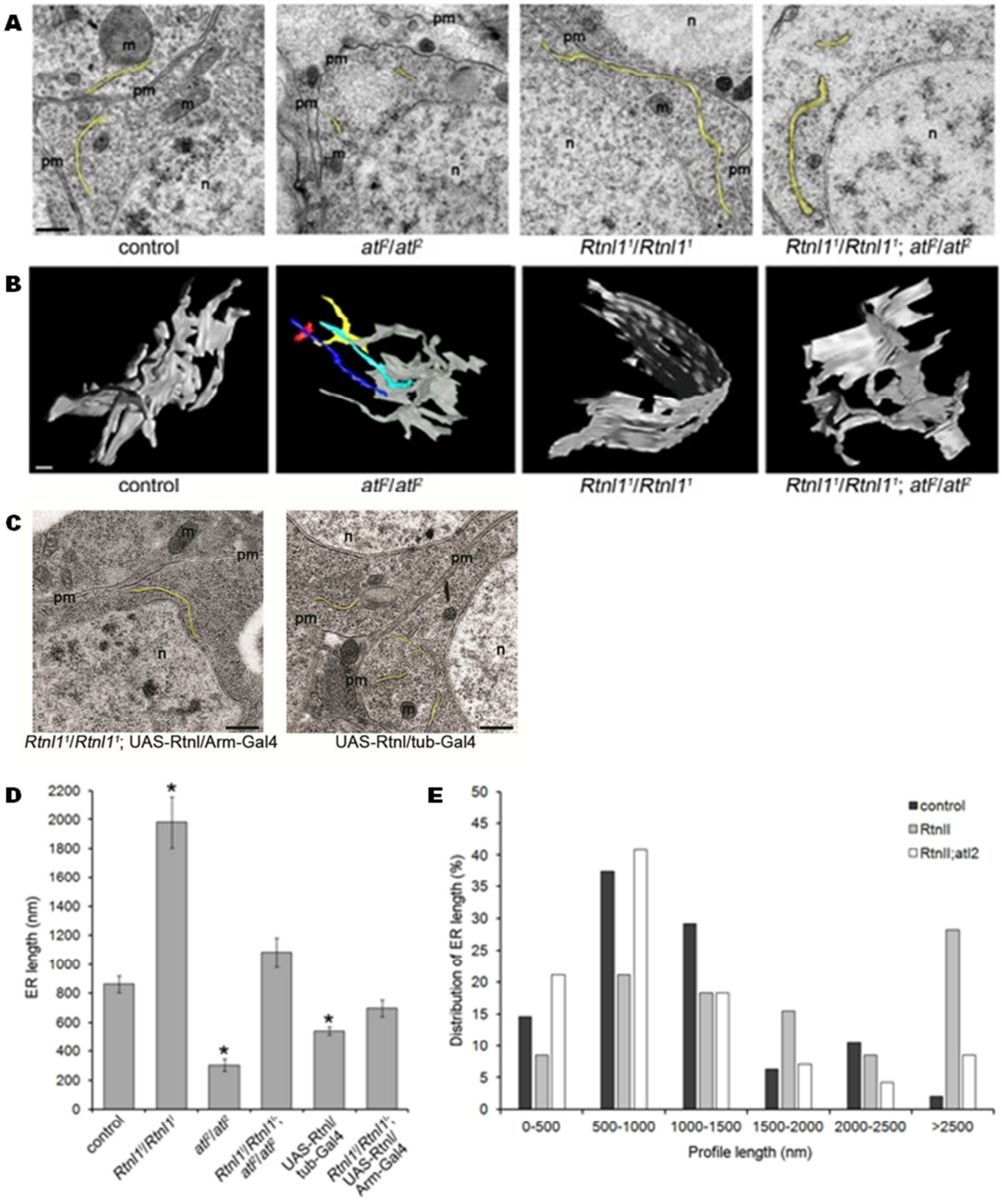

Fig. 12 – Ultrastructural analysis of Rtnl1[1] and atl[2] mutants. (**A**) Representative EM images of ER morphology in larva brain neurons. ER profiles are highlighted. Scale bar:500 nm. pm, plasma membrane; m, mitochondria; n, nucleus. (**B**) EM tomography-based 3D reconstruction of portions of ER network from the indicated genotypes. ER elements not connected are shown in color. Scale bar: 200 nm. (**C**) Left: rescue of Rtnl1[1] mutants by re-expression of transgenic UAS-Rtnl1 under the control of the ubiquitous promoter armadillo-Gal4. Right: EM images of neurons overexpressing Rtnl1 in a wild type background. Scale bar: 500 nm. (**D**) Average length of ER profiles measured on thin EM sections. Error bars represent S.E.M.; n>100; * $p<1x10^{-8}$. (**E**) Size distribution of ER profile length.

3.1.3 Rtnl1 overexpression induces shortening of ER tubules and loss of ER continuity

Since reduction in Rtnl1 levels produced longer ER profiles suggesting a role in membrane fission, we predicted that overexpression of Rtnl1 should cause decrease in ER profile length. To test this hypothesis and to study *in vivo* the effects of Rtnl1 overexpression we used UAS-Rtnl1 transgenic lines. We expressed UAS-HA-Rtnl1 with the ubiquitous driver line tubulin-Gal4 and found that overexpression of Rtnl1 has no apparent phenotypes and the resulting flies are viable and normal by all criteria. To investigate the consequences of Rtnl1 overexpression on ER morphology we applied both confocal and EM. Confocal microscopy analysis of tubulin-Gal4,UAS-GFP-KDEL/UAS-HA-Rtnl1 third instar larva muscles revealed that the normally punctuate fluorescence of the ER marker GFP-KDEL was prominently concentrated in bright punctae enriched especially in the perinuclear region (Fig. 13). This phenotype is reminiscent of the ER fragmentation observed following loss of atlastin function (Orso

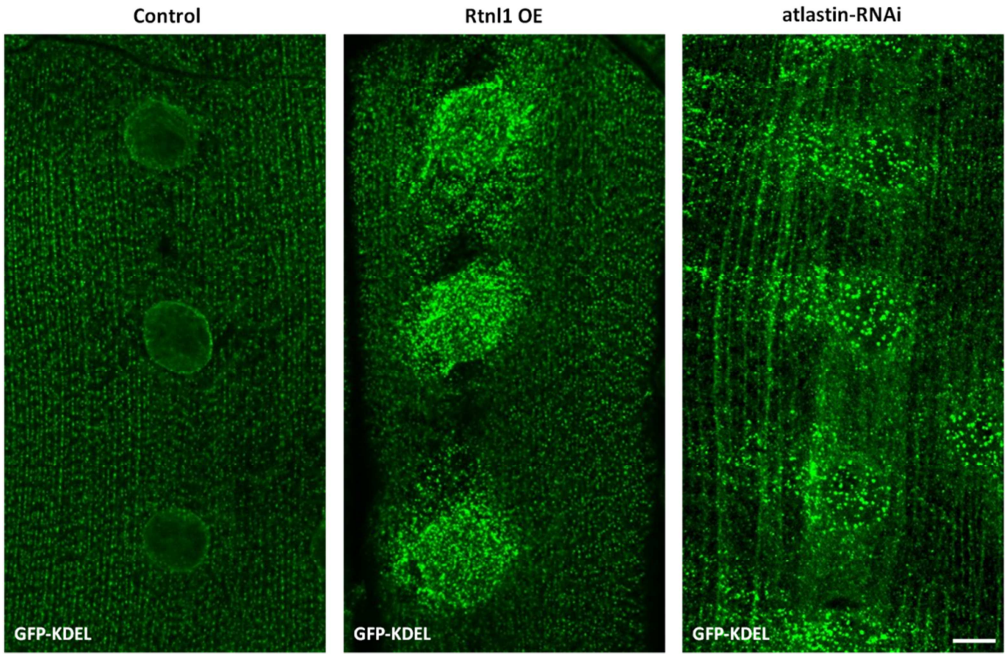

Fig. 13 – Confocal microscopy analysis of controls and tubulin-Gal4,UAS-GFP-KDEL/UAS-HA-Rtnl1 third instar larva muscles. Rtnl1 overexpression (Rtnl1 OE) causes an enrichment of the ER/SR marker GFP-KDEL around the nuclei of third instar larva muscle. A similar phenotype is also produced by loss of atlastin. Scale bar: 10 µm.

et al., 2009; Fig. 13).

To establish whether this apparent morphological change of the ER resulted in loss of luminal continuity we used fluorescence loss in photobleaching (FLIP). We simultaneously expressed Rtnl1 and the luminal marker UAS-GFP-KDEL and photobleached a defined region of a muscle in living larvae. In a normally continuous ER/SR repeated photobleaching of the target area results in decreased fluorescence intensity in neighboring areas due to diffusion of UAS-GFP-KDEL into the bleached area from surrounding tissue. Unlike in control muscle where loss of GFP-KDEL fluorescence was as expected homogeneous in all regions analyzed, repetitive photobleaching of GFP-KDEL in tubulin-Gal4,UAS-GFP-KDEL/UAS-HA-Rtnl1 muscle produced regions of unbleached fluorescence, showing that regions adjacent to the bleached areas did not lose fluoresce over time (Fig. 14). This implies that GFP-KDEL is unable to diffuse and suggests that Rtnl1 overexpression triggers network fragmentation thus interrupting the luminal continuity of the ER.

To investigate ER morphology in greater detail we performed electron microscopy experiments. EM analysis of third instar larva brains overexpressing Rtnl1 established that the average ER profile length was about half (542±28 nm) that of controls (Fig. 12C and D) providing evidence that Rtnl1 overexpression causes shortening of ER profiles.

Shortening of ER elements and loss of ER continuity caused by ectopic expression of Rtnl1 are consistent with fragmentation of the ER caused by increased membrane fission and suggests that Rtnl1 could be a direct mediator of this process.

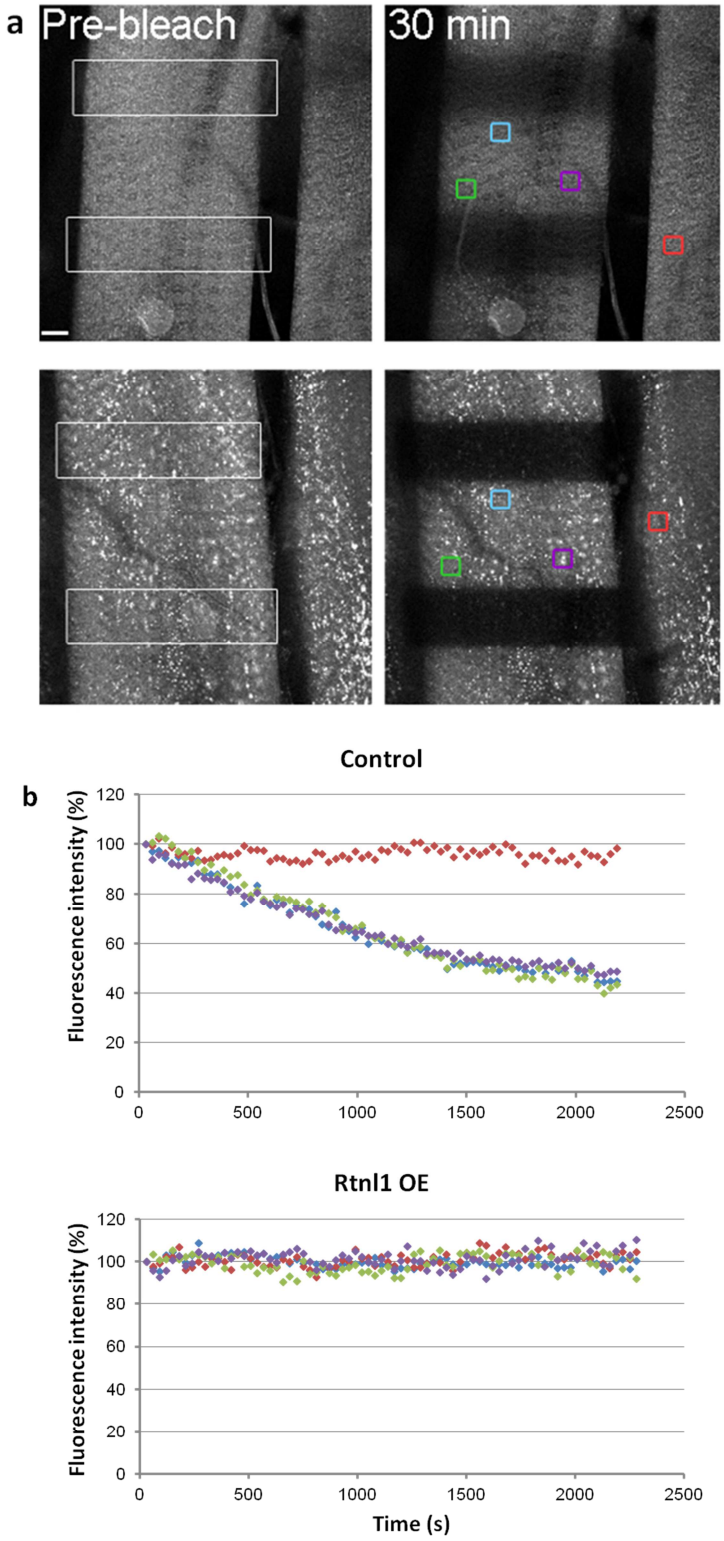

Fig. 14 – Overexpression of Rtnl1 causes fragmentation and discontinuity of the ER. (**a**) FLIP was performed by repetitive photobleaching of two regions (white outline box) in control and Rtnl1 overexpressing (Rtnl1 OE) muscles labeled with GFP-KDEL. Fluorescence loss was analyzed in four independent regions of the muscle (color outline boxes). The red box was chosen on an adjacent unbleached muscle as a control. Scale bar: 10 µm. (**b**) Rates of loss of fluorescence for each boxed area are plotted. In control muscle all ROI lose fluorescence at a similar exponential rate. In contrast, overexpression of Rtnl1 prevents loss of GFP-KDEL fluorescence.

3.1.4 Rtnl1 has membrane fission activity *in vitro*

To verify whether *Drosophila* reticulon has intrinsic membrane fission activity we tested if purified Rtnl1 is sufficient to produce fission when incorporated into pure lipid bilayers. This assay was performed in collaboration with the laboratory of Vadim Frolov at University of Leioa (Spain). To carry out *in vitro* experiments we developed a protocol for the production and purification of Rtnl1 in bacteria (see Methods 2.3.1; Fig. 15).

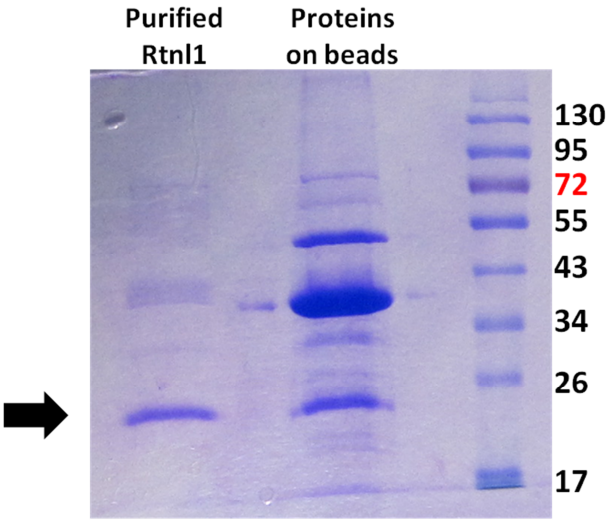

Fig. 15 – Analysis of the Rtnl1 purification. Purification of GST-tagged Rtnl1. Rtnl1 was expressed in bacteria and further purified using GST-affinity beads, the protein was eluted from the beads by digestion with GST-SENP2 protease. The black arrow indicates Rtnl1.

Purified recombinant Rtnl1 was DyLight 488-labeled and reconstituted into 100 nm unilamellar liposomes. Starting from these proteo-liposomes giant unilamellar vesicles (GUVs) were generated. Rtnl1 efficiently incorporated into GUV membranes and produced complex membrane morphologies as well as numerous small buds on the GUV membrane while control GUV lacking the protein did not show the presence of buds (Fig. 16a and b). Interestingly, Rtnl1 accumulated in the places of membrane budding (Fig 16). In larger buds Rtnl1 clusters were visibly associated with the buds neck (Fig 16b), a localization characteristic of membrane fission proteins. Over time small vesicles appeared inside and outside of the GUVs, consistent with membrane fission events. However, the extreme mobility of the buds on the GUV membrane and the relatively slow kinetics of fission complicated the visualization of the actual fission events. Thus, to keep buds in a single focal plane tubes were pulled from Rtnl1-containing GUVs (Fig. 16c). The frequency of bud detachment from the tube was

calculated to obtain an estimation of membrane fission events (Fig. 16d). The fission efficiency of Rtnl1 has been estimated to be 35±15% of buds detached within 30 minutes of observation (7 tubes analyzed), while in the absence of Rtnl1 no spontaneous fission of lipid tubes (n=15) was ever detected within 100 seconds upon tube pulling. Moreover, 4 out 15 tubes containing Rtnl1 broke spontaneously within the observation timeframe (Fig. 17).

These *in vitro* observation corroborate our *in vivo* results implicating Rtnl1 as a mediator of ER membrane fission.

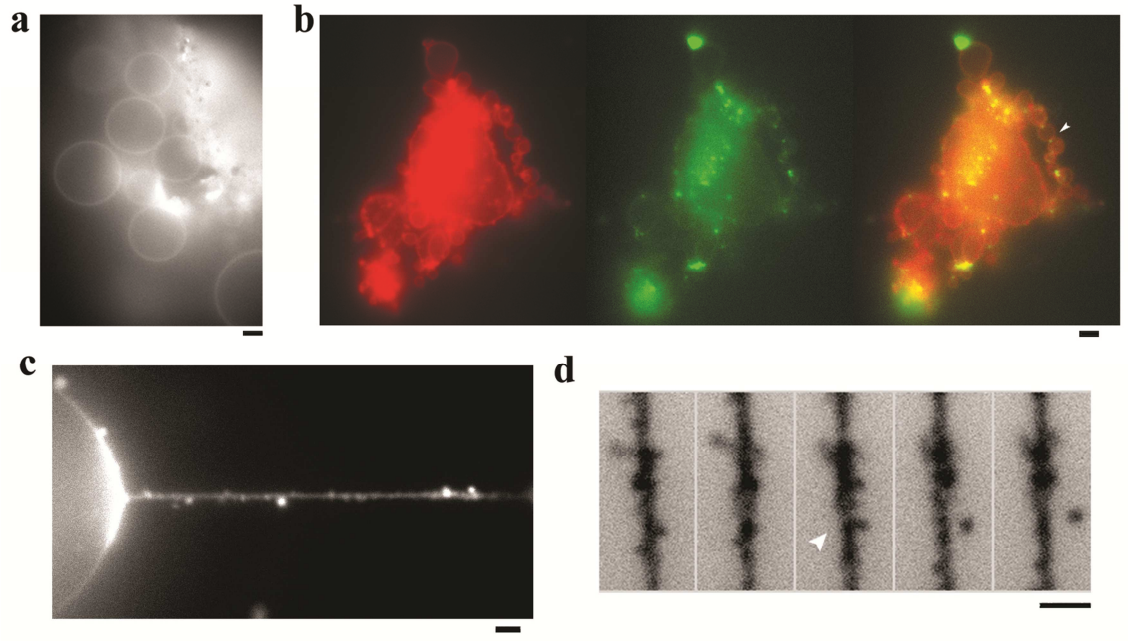

Fig. 16 – Rtnl1 induces membrane fission *in vitro*. (**a**) GUVs produced from 100 nm liposomes. GUV membranes contain fluorescent-labeled lipid (Rh-DOPE). (**b**) GUVs produced from proteo-liposomes containing Rtnl1. Red fluorescence comes from Rh-DOPE, green fluorescence comes from DyLight-488 Rtnl1. Arrow indicates Rtnl1 clusterization on the membrane neck. (**c**) Rtnl1-produced membrane buds on a tube pulled from a Rtnl1-containing GUV. Rh-DOPE fluorescence is shown; small buds produced by Rtnl1 are seen on the tube as well as on the parent GUV. (**d**) the frame sequence (100 ms interval) showing detachment of a vesicles from the membrane tube pulled from a GUV. Rh-DOPE fluorescence is shown, images are inverted for clarity. All bars are 2 µm.

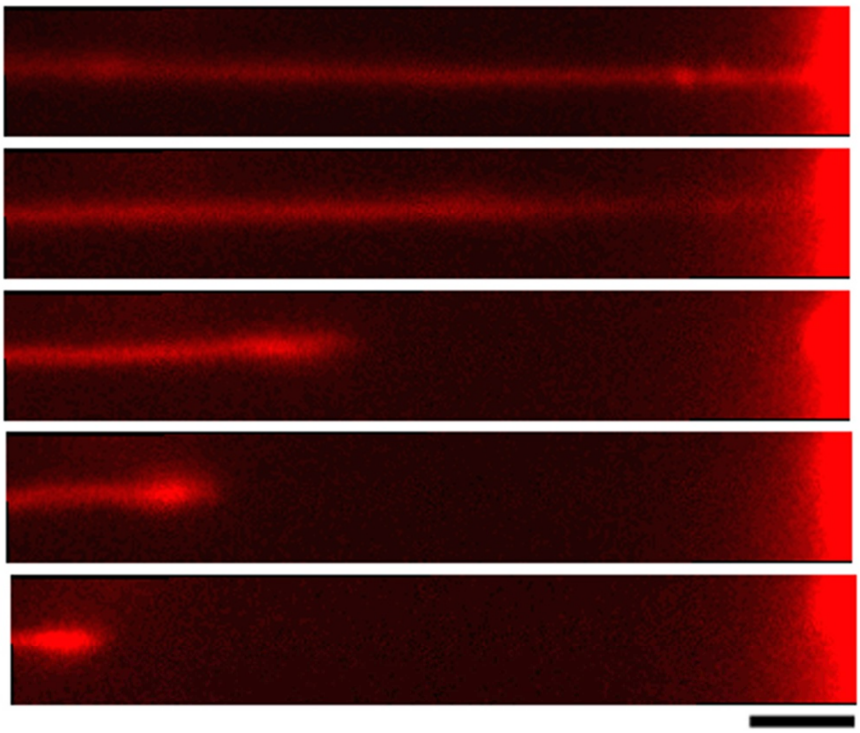

Fig. 17 – Membrane tube pulled from GUVs containing Rtnl1 breaks spontaneously shortly after formation, the breakage occurs at the region containing membrane buds. Scale bar: 2µm.

3.2 DP1

3.2.1 DP1 and atlastin interact genetically

Like reticulon, Deleted in Polyposis protein 1 (DP1) has been implicated in the generation of the tubular ER (see Introduction 1.4). The *Drosophila* genome contains only one highly conserved DP1 ortholog, CG8331, a situation that facilitates the study of this protein.

A physical interaction between atlastin and DP1 has been proposed in yeast (Hu *et al.*, 2009). However, the functional significance of this interaction remains unclear. Thus, we decided to investigate this aspect addressing whether an interaction is present between the *Drosophila* homologs of atlastin and DP1.

First, we generated a construct for the expression of DP1 in cell lines. DP1 cDNA was cloned in the pcDNA3.1/Zeo(+) plasmid in frame with a N-terminal Myc tag. This construct was then transfected in COS-7 cells, both alone and together with a previously generated plasmid for the expression of atlastin in mammalian cells.

Transfection of DP1 in COS-7 cells does not perturb the ER morphology although the protein properly localizes to the ER as shown by its co-localization with the ER marker calnexin (Fig. 18b). In contrast, COS-7 cells transfected with wild-type *Drosophila* atlastin exhibit a disruption of ER morphology, caused by an excessive fusion of ER membranes (Fig. 18a). When DP1 was simultaneously expressed with atlastin we found that over 60% of the cells co-expressing wild type atlastin and DP1 display a morphologically normal ER while 100% of cells expressing only atlastin exhibit the typical overfused ER phenotype (Fig. 18d and e). The observation that DP1 expression suppresses the perturbed ER morphology induced by overexpression of atlastin, strongly suggests that DP1 has the ability to counteract the fusogenic activity of atlastin. Therefore, as reticulon, DP1 appears to be an antagonist of atlastin function.

We confirmed the interaction between atlastin and DP1 in the *Drosophila* eye (Fig. 19). To generate *Drosophila* transgenic lines overexpressing DP1, the DP1 cDNA was cloned in frame with an N-terminal Myc tag in the pUAST vector. This construct was microinjected in *Drosophila* embryos and the resulting transgenic lines were mapped to a specific chromosome and balanced. As described earlier, ectopic expression of atlastin in the developing eye gives rise to a small and rough eye phenotype (Fig. 19c; Orso *et al.*, 2009). In contrast, overexpression of DP1 in the eye does not perturb its external

morphology (Fig. 19b). We reasoned that if atlastin and DP1 function antagonistically, overexpression of DP1 would rescue the atlastin-dependent rough eye phenotype. As predicted, DP1 overexpression in an eye simultaneously expressing atlastin fully restored the normal morphology (Fig. 19d). Together these experiments strongly suggest that in *Drosophila* atlastin and DP1 display a robust antagonistic functional interaction.

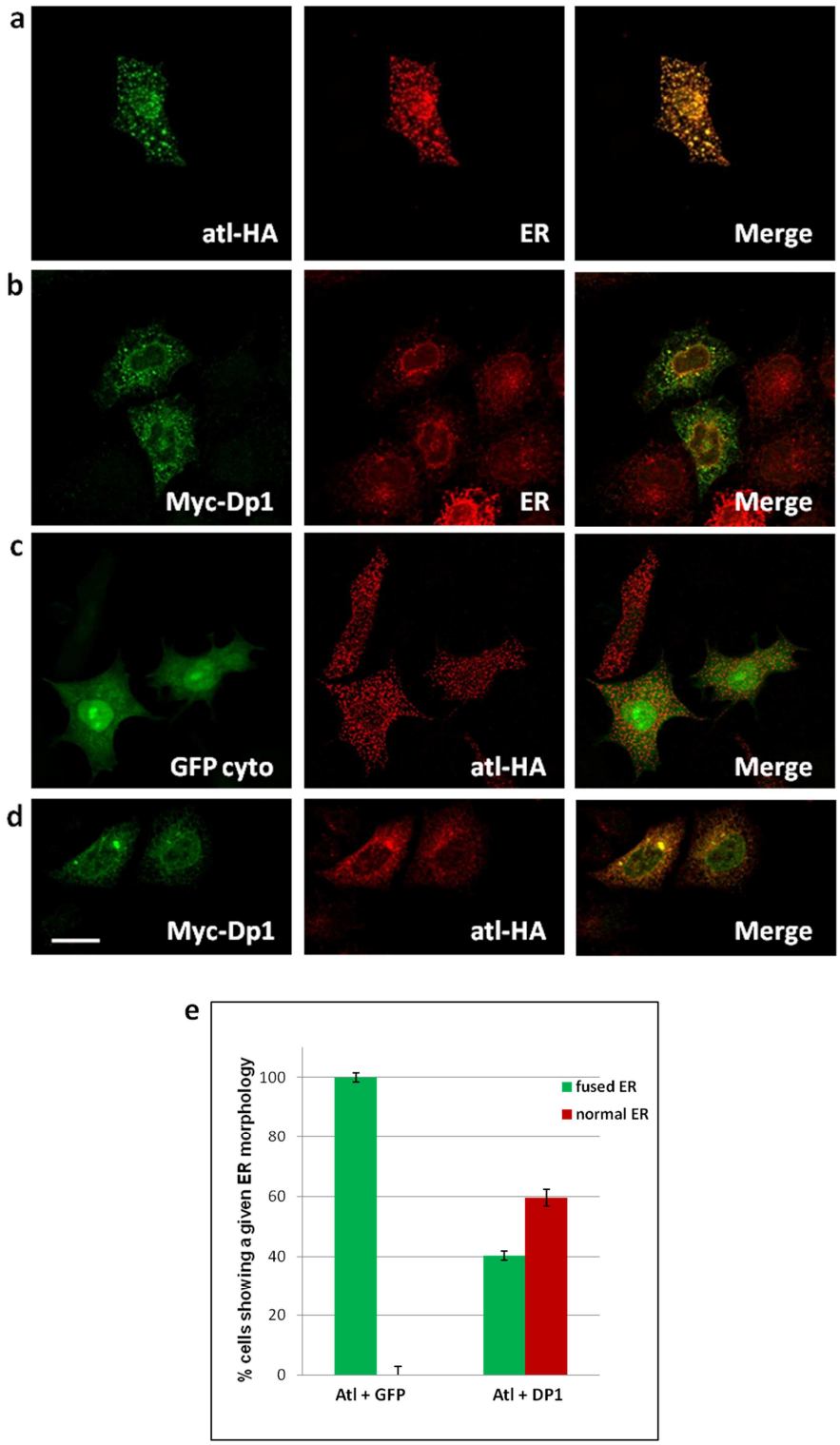

Fig. 18 – Overexpression of DP1 rescues atlastin hyperfusion of ER membranes. (**a**) Overexpression in COS-7 cells of *Drosophila* atlastin-HA (green) induces hyperfusion of ER membranes, as shown by staining with calnexin (red). (**b**) COS-7 cells trasfected with Myc-DP1 (green) shows that it localizes to the ER (red) but does not perturb ER morphology. (**c**) Hyperfusion of ER membranes caused by atlastin-HA (red) is not affected by co-trasfection of a "control protein" (GFP). (**d**) Co-trasfection in COS-7 cells of DP1 (green) and atlastin (red) leads to suppression of the atlastin-dependent hyperfusion phenotype. (**e**) Quantification of atlastin inhibition by co-expression of DP1. Scale bar: 20 µm.

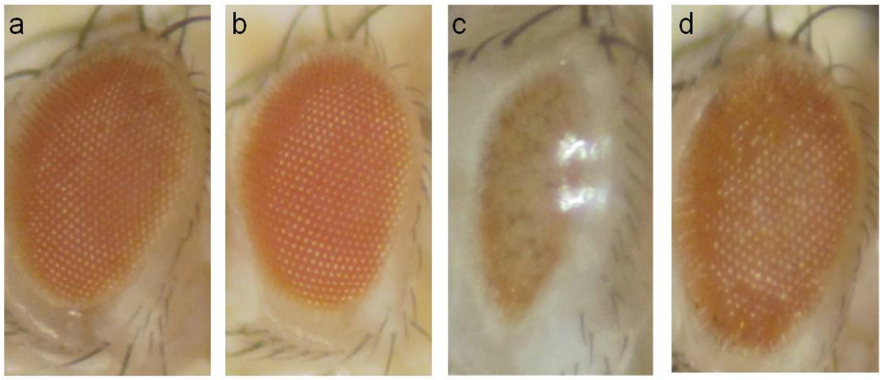

Fig. 19 – *Drosophila* atlastin and DP1 interact genetically. (**a**) Adult *Drosophila* eye (GMR-Gal4/+). (**b**) Eye overexpression of DP1 using GMR-Gal4 does not perturb the eye phenotype (GMR-Gal4/UAS-Myc-DP1). (**c**) Overexpression of atlastin using GMR-Gal4 generates a small eye (GMR-Gal4,UAS-atlastin/+). (**d**) The small eye produced by overexpression of atlastin is rescued by co-expression of DP1 under GMR-Gal4 driver (GMR-Gal4,UAS-atlastin/UAS-Myc-DP1).

3.2.2 *In vivo* analysis of DP1 function

DP1 has been proposed to be implicated in determining the shape of the tubular ER. Considered the antagonistic genetic interaction that we observed between DP1 and atlastin, we extended our analysis in order to understand DP1 role in ER morphogenesis.

Null mutant *Drosophila* lines for DP1 are currently not available. As an alternative loss of function approach we exploited RNAi mediated downregulation. UAS-DP1-RNAi flies are available at the Vienna *Drosophila* RNAi Centre (KK-105290). To determine whether loss of DP1 has phenotypic consequences, we crossed UAS-DP1-RNAi flies with the ubiquitous driver tubulin-Gal4 at 28°C in order to maximize the effect of the RNAi on the transcriptional level of DP1. Examination of the progeny showed that UAS-DP1-RNAi/+;tubulin-Gal4/+ individuals are viable and have no phenotypic abnormalities. To determine the efficacy of *in vivo* RNAi, we tested if the transcriptional level of DP1 is reduced in UAS-DP1-RNAi/+;tubulin-Gal4/+ using quantitative Real-Time PCR (qRT-PCR). Total mRNA was isolated from UAS-DP1-RNAi/+;tubulin-Gal4/+ flies and qRT-PCR was performed. We found that the KK-105290 line causes a 90% reduction of DP1 with respect to wild type control flies, demonstrating that this RNAi efficiently downregulates DP1 (Fig. 20).

We initially performed immunofluorescence experiments on larva muscles lacking or overexpressing DP1 to examine ER integrity *in vivo* using the ER marker GFP-KDEL.

To do this, we crossed UAS-DP1-RNAi/+ or UAS-Myc-DP1/+ flies with the ubiquitous driver tubulin-Gal4,UAS-GFP-KDEL/+.

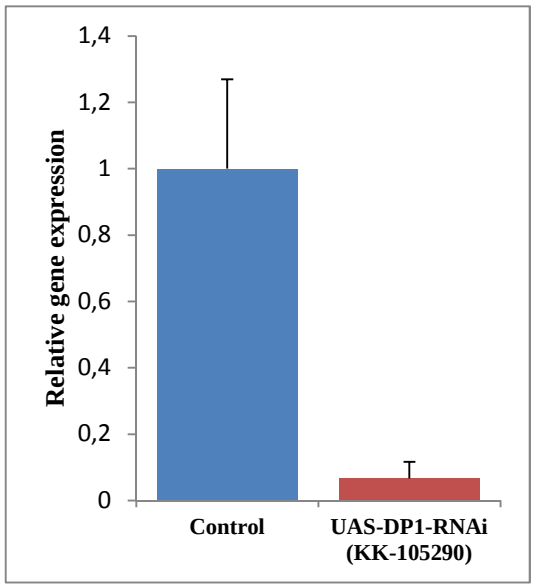

Fig. 20 – Bar graph illustrating real time PCR data demonstrating the reduction of DP1 mRNA levels in UAS-DP1-RNAi/+;tubulin-Gal4/+ flies. Assays were performed in triplicate and results shown are representative of two independent experiments.

We did not observe any differences in the distribution or localization of the ER/SR marker between *Drosophila* muscles lacking or overexpressing DP1 and control muscles (Fig. 21). Therefore, we decided to perform electron microscopy (EM) analysis to assess the morphology of the ER in greater detail in ventral nerve chord neurons of third instar larva brains. Ultrastructural analysis of the ER revealed significant morphological differences in the ER in neurons of UAS-DP1-RNAi flies compared to controls (Fig. 22). Indeed, ER profiles of UAS-DP1-RNAi neurons display an alteration of ER length compared to ER profiles of wild type neurons (Fig 22). ER profiles in control neurons have an average length of 702±33 nm, whereas neurons lacking DP1 showed elongated ER profiles (1161±81 nm). In contrast, ultrastructural analysis of the ER of neurons overexpressing DP1 did not show any significant changes in profile length or morphology (Fig. 22).

Although still preliminary, these results suggest that DP1 influences ER morphology in *Drosophila* and its antagonistic interaction with atlastin suggests that DP1 might function in a manner analogous to that of Rtnl1. Nevertheless, DP1 activity will clearly need further in depth characterization before we can extend our conclusions.

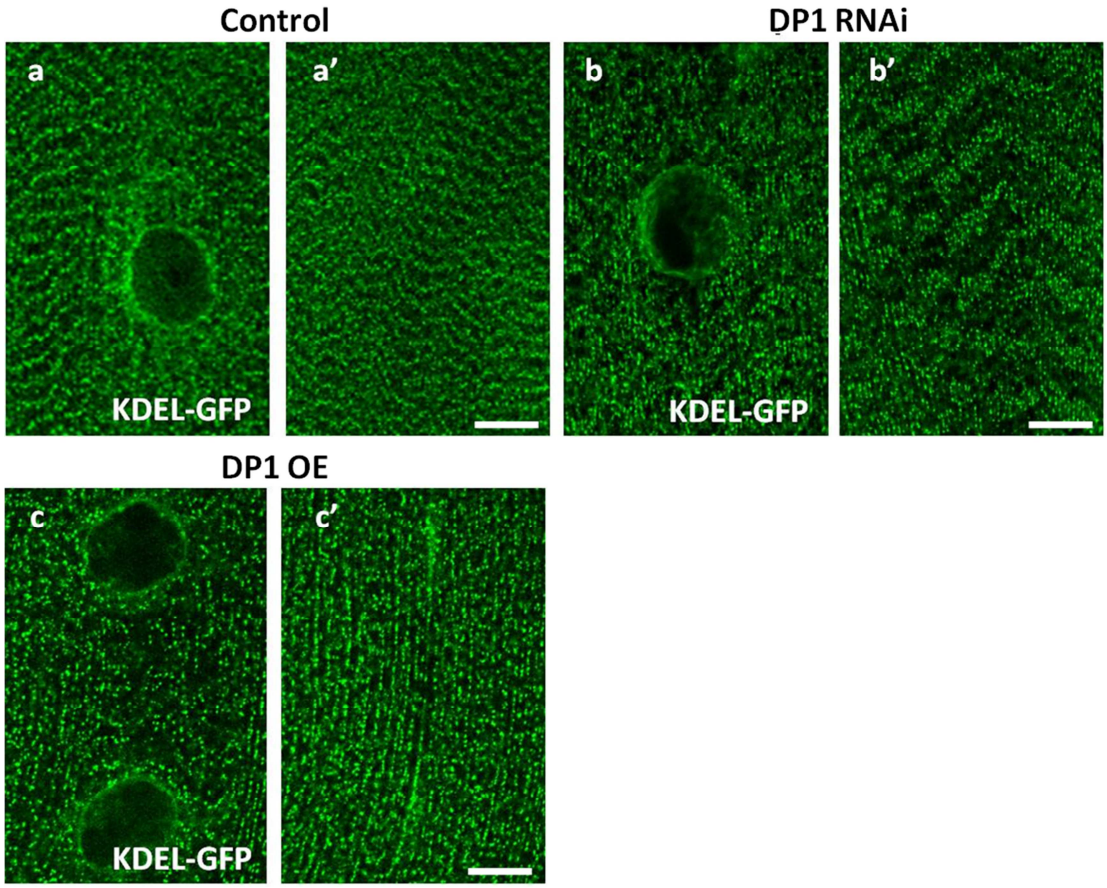

Fig. 21 – Knock down and overexpression of DP1 protein in *Drosophila* did not show significant morphological alterations of the ER/SR structure. Fluorescence confocal microscopy analysis were carried out on muscle 6 or 7 of the abdominal segment 2 on third instar larvae overexpressing DP1 (DP1 OE) or knocked down for DP1 expression (DP1 RNAi). We used the GFP-KDEL as a marker for labeling the ER/SR structure. **a-a'**) tubulin-Gal4,UAS-GFP-KDEL/+ body wall muscles. **b-b'**) UAS-DP1-RNAi/+;tubulin-Gal4,UAS-GFP-KDEL/+ body wall muscles: the morphology of the ER/SR appears normal if compared to controls. **c-c'**) UAS-Myc-DP1/+;tubulin-Gal4,UAS-GFP-KDEL/+ body wall muscles. Scale bar: 10 µm.

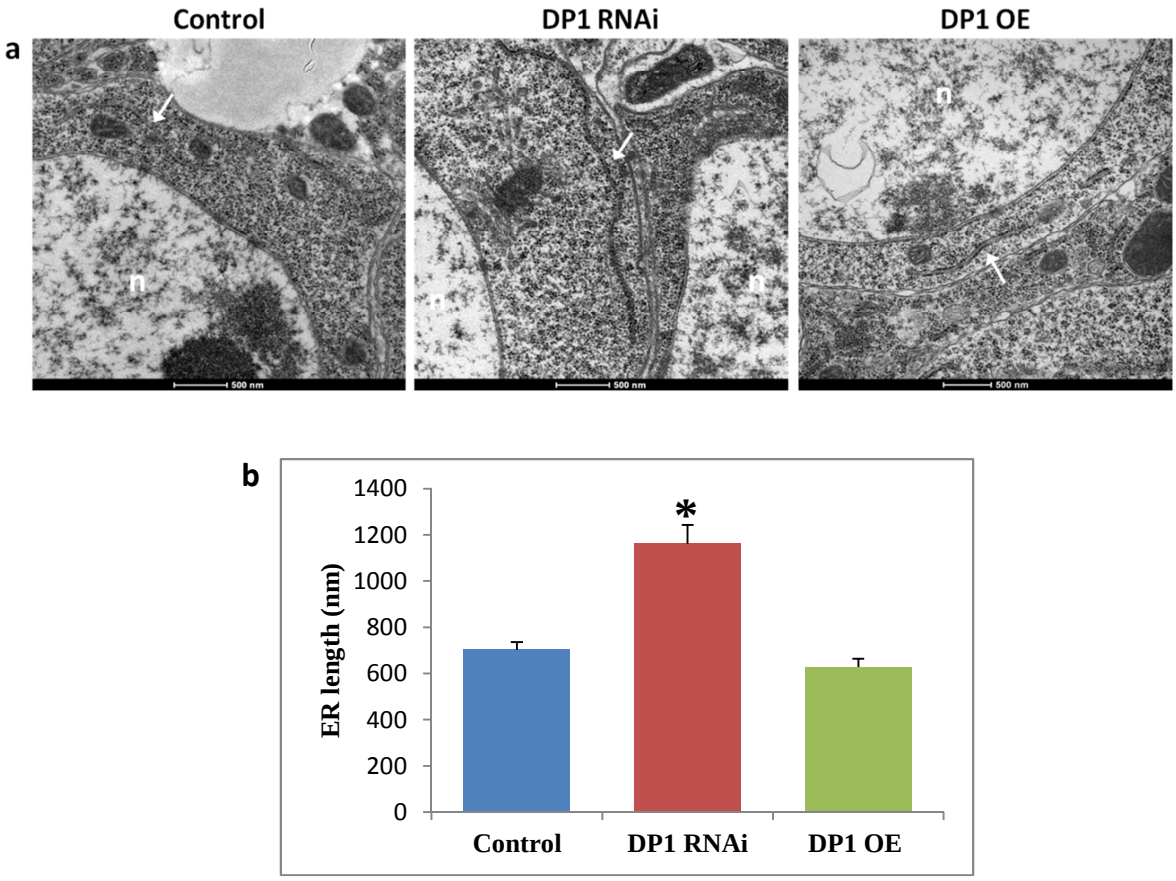

Fig. 22 – Ultrastructural analysis of tissues lacking or overexpressing DP1. (**a**) Representative EM images of ER morphology in larva brain neurons. White arrows indicate ER; "n" indicates nucleus. Scale bar:500 nm. (**b**) Average length of ER profiles measured on thin EM sections. Error bars represent S.E.M.; n>100; * $p<1x10^{-9}$.

4 DISCUSSION

The Endoplasmic reticulum (ER) forms an elaborate and extensive network that spreads throughout the cell. Establishment and maintenance of proper architecture is essential for endoplasmic reticulum function. The ER is a highly dynamic network whose overall architecture is thought to be maintained by specialized proteins that control membrane curvature and by a balance between membrane fusion and fission (Pendin *et al.*, 2011). Homotypic fusion occurs when two initially separate membrane merge into a single one. It has been demonstrated that *Drosophila* atlastin, the fly homologue of the GTPase atlastin-1, mediates membrane tethering and fusion of ER membranes (Orso *et al*., 2009). On the contrary, membrane fission splits an initially continuous membrane into two separate ones. This process is crucial for the maintenance and the function of all cellular membranes that require the breaking of membranes such as exocytosis, mitochondria division, cell division. Although there are no evidence *in vivo* for ER membrane fission, several clues suggest that this process is likely to operate in the cell. Indeed, ER fragmentation has been documented in neurons (Kucharz *et al.*, 2009) and, albeit controversial, disassembly of the ER during mitosis is also reported (Du *et al.*, 2004). These observations suggest that the cells have the ability to actively break ER membranes and this ability should depend on proteins that drive or facilitate membrane fission. However, such ER fission or fission-permissive proteins have not been identified.

The reticulons and DP1/REEP/Yop1 are a class of highly conserved, integral ER membrane proteins thought to be involved in the morphogenesis of ER tubules (Voeltz *et al.*, 2006). It has been demonstrated that mutations in both reticulon 2 and atlastin-1 are linked to the neurodegenerative disorder hereditary spastic paraplegia and that mutations of *SPG31* gene, which encodes REEP1 protein that belongs to the DP1/REEP/Yop1 superfamily, are responsible for a dominant form of hereditary spastic paraplegia.

In this work we used *Drosophila melanogaster* as a model organism to study the function of Rtnl1 and DP1 in maintaining and determining the morphology of endoplasmic reticulum. The presence in the *Drosophila* genome of a single high conserved Rtnl1 and DP1 ortholog combined with the wide array of experimental tools available, makes *Drosophila* a valuable system to investigate potential genetic and/or functional interactions between atlastin, Rtnl1 and DP1.

Here we find that in *Drosophila* Rtnl1 and atlastin interact genetically in an antagonistic manner and that modulation of Rtnl1 expression *in vivo* markedly affects atlastin loss and gain of function phenotypes. Indeed, we demonstrate that genetic elimination of Rtnl1 in the atlastin null background rescues the lethality associated with depletion of atlastin and fully recuperates ER fragmentation, showing that the fragmentation observed upon loss of atlastin function is likely due to the activity of Rtnl1. Moreover, we show that in the fly eye knockdown of Rtnl1 results in enhancement of the small eye produced by atlastin overexpression. This strong, antagonistic genetic interaction between *atlastin* and *Rtnl1* suggests that the encoded proteins exert opposing functions in the control of ER architecture. We propose that in the ER Rtnl1 complements atlastin-mediated fusion by promoting membrane fission. Consistent with this hypothesis, we find that loss of Rtnl1 causes elongation of ER profiles while overexpression of Rtnl1 produces shorter profiles. FLIP analysis suggests that the ER lumen is discontinuous in *Drosophila* tissues overexpressing Rtnl1, further corroborating the hypothesis that Rtnl1 has a role in breaking membranes. These *in vivo* data support the hypothesis that Rtnl1 functions to counterbalance atlastin fusogenic activity by mediating membrane fission to dynamically maintain overall ER morphology.

The intrinsic membrane fission ability of Rtnl1 is also suggested by reconstitution of the protein into pure lipid bilayers. Indeed, experiments performed *in vitro* indicate that Rtnl1 is sufficient to drive the release of membrane vesicles from lipid bilayers similar, albeit less efficiently, to the prototype fission protein dynamin-1 (Pucadyil & Schmid, 2008). As dynamin-1, Rtnl1 forms clusters specifically in the necks of membrane buds. Formation of stable clusters invokes the general ability of reticulons to oligomerize *in vivo* (Shibata *et al.*, 2008). When assembled on a vesicles neck such clusters would impose saddle-like membrane curvature that is a general precursor of membrane fission (Kozlov *et al.*, 2010). Moreover, the membrane incorporation of Rtnl1 *in vitro* is greatly improved by cholesterol. The dependence of Rtnl1 membrane incorporation on cholesterol suggests that the transmembrane portion of Rtnl1, similarly to that of caveolin, could sequester cholesterol. Accumulation of cholesterol in the necks of budding vesicles has long been associated with membrane fission (Schmid & Frolov, 2011). Together, these observations indicate that Rtnl1 potentially integrates key elements of a general membrane scission machinery. However, important differences set Rtnl1 apart from dynamin-1. Dynamin-1 requires the energy provided by hydrolysis

of GTP to break the membrane in an active, energy-dependent manner. Rtnl1, in contrast, does not use a source of energy and relies on its ability to bend membranes to induce extreme curvature and close vicinity of the two monolayers. This vicinity in turn would favor breakage of the membrane by the intrinsic instability of lipids thus permitting membrane scission. The reliance on energy is also the reason why dynamin-1 mediates fission much more efficiently. We therefore propose that while dynamin-1 is an active fission machinery, Rtnl1 has a permissive role in this process. Further studies will be necessary to analyze the precise mechanism underlying the ability of Rtnl1 to mediate breaking of ER membranes.

Another family of proteins related to the reticulons is that comprising the DP1/REEP/Yop1 proteins. The reticulons do not share any primary sequence homology with members of the DP1/REEP/Yop1 family, however, both families contain a conserved domain characterized by the presence of two long hydrophobic segments, the reticulon homology domain (RHD). DP1/REEP/Yop1 require the RHD domain for their proper insertion in the ER membrane (Shibata *et al.*, 2008). It has been proposed that DP1/REEP/Yop1 proteins deform the lipid bilayer into high-curvature tubules through hydrophobic insertion and scaffolding mechanisms by occupying more space in the outer than the inner leaflet of the ER lipid bilayer *via* their membrane-inserted, double-hairpin hydrophobic domains (Hu *et al.*, 2009). DP1, as Rtnl1, includes two hydrophobic regions conferring a “wedge” shape to the protein that shallowly inserts into the outer lipid monolayer of the ER membrane.

Our initial studies of DP1 in *Drosophila* suggest that an antagonistic genetic interaction exists also between DP1 and atlastin. Indeed, we found that in the fly eye, overexpression of DP1 rescues the small eye produced by atlastin overexpression and in COS-7 cells the excessive ER fusion caused by trasfected atlastin is suppressed by co-expression of DP1. A physical interaction between atlastin and DP1 in yeast has been demonstrated by Hu and colleagues that proposed that atlastin and DP1 cooperate in the formation of tubular ER network (Hu *et al.*, 2009). Moreover, previous work has suggested that DP1 plays a role in shaping the ER membranes (Hu *et al.*, 2008; Shibata *et al.*, 2008; Voeltz *et al.*, 2006). Our results indicate that also in *Drosophila* DP1 influences the morphology of the ER since we found that neurons lacking DP1 display an elongation of the ER profiles.

The strong antagonistic genetic interaction between atlastin and DP1 and the alteration of the ER profiles in neurons lacking DP1 are reminiscent of results that we obtained

with Rtnl1 but are in stark contrast with the cooperative role between atlastin and reticulon described in yeast. Although further studies are necessary, we surmise that in our system Rtnl1 and DP1 may have a redundant function in regulating the structure of the ER. While for Rtnl1 our data show that this protein has an intrinsic ability to facilitate membrane fission, a similar conclusion cannot be reached yet for DP1 since, for example, data on the *in vitro* activity are still lacking. However, the observations that DP1 antagonizes atlastin and that its loss leads to an elongated ER suggest that DP1 could have a function analogous to that of Rtnl1. This would in turn suggest that in order to maintain the general structure of the ER network membrane fusion mediated by atlastin is counterbalanced by the activity of two or possibly more proteins. It has been demonstrated that the RHD domain is the crucial region of reticulon and DP1. This domain is in fact responsible for the wedging mechanism underlying the curvature potential of these proteins (Shibata *et al.*, 2008; Hu *et al.*, 2008). Our proposition is that proteins containing this domain, such as reticulons and DP1/REEP/Yop1 proteins, have an intrinsic ability to break ER membranes due to their capacity to induce extreme curvature of the bilayers. Areas of extreme curvature can potentially be the site of membrane scission because of the intrinsic instability of lipids.

Although ER membrane fission/scission has not been documented directly, this work intimates that indeed a balance between membrane fusion and scission events is required to maintain the overall structure of the ER network. While the potent membrane fusion action of atlastin leads to increased network complexity, simplification of the network is possibly achieved through the functionally antagonistic protein membrane remodeling activity of reticulon and possibly other proteins including DP1. It has been proposed that another mechanism leading to simplification of the network in yeast involves loss of tubular ER polygons, potentially mediated by Lunapark (Lnp1p), a protein that in yeast counteracts the activity of the atlastin homolog Sey1p (Chen *et al.*, 2012). Although the role of Lunapark in higher organisms is not clear, it is entirely possible that different mechanisms contribute to counterbalance ER fusion.

5 REFERENCES

Anderson D. & Hetzer M. (2008) – Reshaping of the endoplasmic reticulum limits the rate for nuclear envelope formation. *J Cell Biol.* 182, 911-924.

Bannai H., Inoue T., Nakayama T., Hattori M., Mikoshiba K. (2004) – Kinesin dependent, rapid, bi-directional transport of ER sub-compartment in dendrites of hippocampal neurons. *J Cell Sci.* 117, 163-75.

Bashkirov P.V., Akimov S.A., Evseey A.I., Schmid S.L., Zimmerberg J., Frolov V.A. (2008) – GTPase cycle of dynamin is coupled to membrane squeeze and release, leading to spontaneous fission. *Cell.* 135, 1276-1286.

Benyamini P., Webster P., Meyer D.I. (2009) – Knockdown of p180 eliminates the terminal differentiation of a secretory cell line. *Mol Biol Cell.* 20, 732-744.

Bian X., Klemm R.W., Liu T.Y., Zhang M., Sun S., Sui X., Liu X., Rapoport T.A., Hu J. (2011) – Structures of the atlastin GTPase provide insight into homotypic fusion of endoplasmic reticulum membranes. *Proc Natl Acad Sci U S A.* 108, 3976-81.

Brand A. H. & Perrimon N. (1993) – Targeted gene expression as a means of altering cell fates and generating dominant phenotypes. *Development.* 118, 401-15.

Byrnes L.J. & Sondermann H. (2011) – Structural basis for the nucleotide-dependent dimerization of the large G protein atlastin-1/SPG3A. *Proc Natl Acad Sci U S A.* 108, 2216-21.

Byrnes L.J., Singh A., Szeto K., Benvin N.M., O'Donnell J.P., Zipfel W.R., Sondermann H. (2013) – Structural basis for conformational switching and GTP loading of the large G protein atlastin. *EMBO J.* 32, 369-384.

Cauchi R.J. & van den Heuvel M. (2006) – The fly as a model for neurodegenerative diseases: is it worth the jump? *Neurodegener Dis.* 3, 338-56.

Chan D.C. (2012) – Fusion and fission: interlinked processes critical for mitochondrial health. *Annu Rev Genet.* 46, 265-287.

Chan H.Y. & Bonini N.M. (2000) – *Drosophila* models of human neurodegenerative disease. *Cell Death Differ.* 7, 1075-80.

Chappie J.S. & Dyda F. (2013) – Building a fission machine – structural insights into dynamin assembly and activation. *J Cell Sci.* 126, 2773-2784.

Chen S., Novick P., Ferro-Novick S. (2012) – ER network formation requires a balance of the dynamin-like GTPase Sey1p and the Lunapark family member Lnp1p. *Nat Cell Biol.* 14, 707-716.

Chen S., Novick P., Ferro-Novick S. (2013) – ER structure and function. *Curr Opin Cell Biol.* 25, 428-33.

Collins R.N. (2006) – How the ER stays in shape. *Cell.* 124, 464-466.

Dayel M.J. & Verkman A.S. (1999) – Diffusion of green fluorescent protein in the aqueous-phase lumen of the endoplasmic reticulum. *Biophys J.* 76, 2843-2851.

De Craene J.O., Coleman J., Estrada de Martin P., Pypaert M., Anderson S., Yates J.R, Ferro Novick S., Novick P. (2006) – Rtn1p is involved in structuring the cortical endoplasmic reticulum. *Mol Biol Cell.* 17, 3009-3020.

Di Sano F., Bernardoni P., Piacentini M. (2012) – The reticulons: guardians of the structure and function of the endoplasmic reticulum. *Exp Cell Res.* 318, 1201-7.

Dreier L. & Rapoport T.A. (2000) – *In vitro* formation of the endoplasmic reticulum occurs independently of a microtubules by controlled fusion reaction. *J Cell Biol.* 148, 883-898.

Du Y., Ferro-Novick S., Novick P. (2004) – Dynamics and inheritance of the endoplasmic reticulum. *J Cell Sci.* 117, 2871-8.

Ellenberg J., Siggia E.D., Moreira J.E., Smith C.L., Presley J.F., Worman H.J., Lippincott-Schwartz J. (1997) – Nuclear membrane dynamics and reassembly in living cells: targeting of inner nuclear membrane protein in interphase and mitosis. *J Cell Biol.* 138, 1193-1206.

English A.R. & Voeltz G.K. (2013) – Rab10 GTPase regulates ER dynamics and morphology. *Nat Cell Biol.* 15, 169-178.

Farhan H. & Hauri H.P. (2009) – Membrane biogenesis: networking at the ER with atlastin. *Curr Biol.* 19, 906-8.

Fassier C., Hutt J.A., Scholpp S., Lumsden A., Giros B., Nothias F., Schneider-Maunoury S., Houart C., Hazan J. (2010) – Zebrafish atlastin controls motility and spinal motor axon architecture *via* inhibition of the BMP pathway. *Nat Neurosci.* 13, 1380-7.

Friedman J.R., Webster B.M., Mastronarde D.N., Verhey K.J., Voeltz G.K. (2010) – ER sliding dynamics and ER-mitochondrial contacts occur on acetylated microtubules. *J Cell Biol.* 190, 363-375.

Goyal U. & Blackstone C. (2013) – Untangling the web: mechanisms underlying ER network formation. *Biochim Biophys Acta.* 1833, 2492-8.

Graham T.R. & Kozlov M.M. (2010) – Interplay of proteins and lipids in generating membrane curvature. *Curr Opin Cell Biol.* 22, 430-6.

Griffing L.R. (2010) – Networking in the endoplasmic reticulum. *Biochem Soc Trans.* 38, 747-753.

Grigoriev I., Gouveia S.M., van der Vaart B., Demmers J., Smyth J.T., Honnappa S., Splinter D., Steinmetz M.O., Putney J.W., Hoogenraad C.C., Akhmanova A. (2008) – STIM1 is a MT-plus-end-tracking protein involved in remodeling of the ER. *Curr Biol.* 18, 177-182.

Hu J., Shibata Y., Voss C., Shemesh T., Li Z., Coughlin M., Kozlov M.M., Rapoport T.A., Prinz W.A. (2008) – Membrane proteins of the endoplasmic reticulum induce high-curvature tubules. *Science.* 319, 1247-50.

Hu J., Shibata Y., Zhu P.P., Voss C., Rismanchi N., Prinz W.A. Rapoport T.A., Blackstone C. (2009) – A class of dynamin-like GTPases involved in the generation of the tubular ER network. *Cell.* 138, 549-561.

Hu J., Prinz W.A., Rapoport T.A. (2011) – Weaving the web of ER tubules. *Cell.* 147, 1226-1231.

Jackson G.R. (2008) – Guide to understanding *Drosophila* models of neurodegenerative diseases. *PLoS Biol.* 6, 53.

Koch G.L., Booth C., Wooding F.B. (1988) – Dissociation and re-assembly of the endoplasmic reticulum in live cells. *J Cell Sci.* 91, 511-522.

Kozlov M.M., McMahon H.T., Chernomordik L.V. (2010) – Protein-driven membrane stresses in fusion and fission. *Trends Biochem Sci.* 35, 699-706.

Kozlovsky Y. & Kozlov M.M. (2003) – Membrane fission: model for intermediate structures. *Biophys J.* 85, 85-96.

Kucharz K., Krogh M. Ng A.N., Torreson H. (2009) – NMDA receptor stimulation induces reversible fission of the neuronal endoplasmic reticulum. *PLoS One.* 4, 5250.

Iwahashi J., Hamada N., Watanabe H. (2007) – Two hydrophobic segments of the RTN1 family determine the ER localization and retention. *Biochem Biophys Res Commun.* 335, 508-512.

Lazar N.L., Singh S., Paton T., Clapcote S.J., Gondo Y., Fukumura R., Roder J.C., Cain D.P. (2011) – Missense mutation of the reticulon-4 receptor alters spatial memory and social interaction in mice. *Behav Brain Res.* 10, 73-9.

Lee M., Paik S.K., Lee M.J., Kim Y.K., Kim S., Nahm M., Oh S.J., Kim H.M., Yim J., Lee C.J., Bae Y.C., Lee S. (2009) – *Drosophila* Atlastin regulates the stability of muscle microtubules and is required for synapse development. *Dev Biol.* 330, 250-262.

Lin S., Sun S., Hu J. (2012) – Molecular basis for sculpting the endoplasmic reticulum membrane. *Int J Biochem Cell Biol.* 44, 1436-1443.

Liu T., Bian X., Sun S., Hu X., Klemm R.X., Prinz W.A., Rapoport T.A., Hu J. (2012) – Lipid interaction of the C terminus and association of the transmembrane segments facilitate atlastin-mediated homotypic endoplasmic reticulum fusion. *Proc Natl Acad Sci U S A.* 109, 2146-54.

Martens S. & McMahon H.T. (2008) – Mechanisms of membrane fusion: disparate players and common principles. *Nat Rev Mol Cell Biol.* 9, 543-56.

McMahon H.T. & Gallop J.L. (2005) – Membrane curvature and mechanisms of dynamic cell membrane remodeling. *Nature.* 1, 590-6.

Mim C. & Unger V.M. (2012) – Membrane curvature and its generation by BAR proteins. *Trends Biochem Sci.* 37, 526-33.

Montenegro G., Rebelo A.P., Connell J., Allison R., Babalini C., D'Aloia M., Montieri P., Schüle R., Ishiura H., Price J., Strickland A., Gonzalez M.A., Baumbach-Reardon L., Deconinck T., Huang J., Bernardi G., Vance J.M., Rogers M.T., Tsuji S., De Jonghe P., Pericak-Vance M.A., Schöls L., Orlacchio A., Reid E., Züchner S. (2012) – Mutations in the ER-shaping protein reticulon 2 cause the axon-degenerative disorder hereditary spastic paraplegia type 12. *J Clin Invest.* 122, 538-44.

Moss T.J., Daga A., McNew J. (2011) – Fusing a lasting relationship between ER tubules. *Trends Cell Biol.* 21, 416-23.

Namekawa M., Muriel M.P., Janer A., Latouche M., Dauphin A., Debeir T., Martin E., Duyckaerts C., Prigent A., Depienne C., Sittler A., Brice A., Ruberg M. (2007) – Mutations in the SPG3A gene encoding the GTPase atlastin interfere with vesicle trafficking in the ER/Golgi interface and Golgi morphogenesis. *Mol Cell Neurosci.* 35, 1-13.

Oertle T., Klinger M., Stuermer C.A., Schwab M.E. (2003) – A reticular rhapsody: phylogenic evolution and nomenclature of the RTNL/Nogo gene family. *FASEB J.* 17, 1238-1247.

O'Sullivan N.C., Jahn T.R., Reid E., O'Kane C.J. (2012) – Reticulon-like 1, the *Drosophila* orthologue of the hereditary spastic paraplegia gene reticulon 2, is required for organization of endoplasmic reticulum and of distal motor axons. *Hum Mol Genet.* 21, 3356-3365.

Orso G., Pendin D., Liu S., Tosetto J., Moss T.J., Faust J.E. Micaroni M., Egorova A., Martinuzzi A., McNew J.A., Daga A. (2009) – Homotypic fusion of ER membranes requires the dynamin-like GTPase atlastin. *Nature.* 460, 978-983.

Pendin D., McNew J.A., Daga A (2011a) – Balancing ER dynamics: shaping, bending, severing and mending membranes. *Curr Opin Cell Biol.* 23, 435-442.

Pendin D., Tosetto J., Moss T.J., Andreazza C., Moro S., McNew J.A., Daga A. (2011b) – GTP-dependent packing of a three-helix bundle is required for atlastin-mediated fusion. *Proc Natl Acad Sci U S A.* 108, 16283-8.

Praefcke G.J. & McMahon H.T. (2004) – The dynamin superfamily: universal membrane tubulation and fission molecules? *Nat Rev Mol Cell Biol.* 5, 133-47.

Prinz W.A., Grzyb L., Veenhuis M., Kahana J.A., Silver P.A., Rapoport T.A. (2000) – Mutants affecting the structure of the cortical endoplasmic reticulum in *Saccharomyces cerevisiae*. *J Cell Biol.* 150, 461-474.

Pucadyil T.J. & Schmid S.L. (2008) – Real-time visualization of dynamin-catalyzed membrane fission and vesicle release. *Cell.* 135, 1263-75.

Puhka M., Vihinen H., Joensuu M., Jokitalo E. (2007) – Endoplasmic reticulum remains continuous and undergoes sheet-to-tubule transformation during cell division in mammalian cells. *J Cell Biol.* 179, 895-909.

Rismanchi N., Soderblom C., Stadler J., Zhu P.P., Blackstone C (2008) – Atlastin GTPases are required for Golgi apparatus and ER morphogenesis. *Hum Mol Genet.* 17, 1591-604.

Roux A. (2014) – Reaching a consensus on the mechanism of dynamin? *Prime Rep.* 6, 86.

Schmid S.L. & Frolov V.A. (2011) – Dynamin: functional design of a membrane fission catalyst. *Annu Rev Cell Dev Biol.* 27, 79-105.

Saini S.G., Liu C., Zhang P., Lee T.H. (2014) – Membrane tethering by the atlastin GTPase depends on GTP hydrolysis but not on forming the cross-over configuration. *Mol Biol Cell.* 25, 3942-3953.

Shibata Y., Voss C., Rist J.M., Hu J., Rapoport T.A., Prinz W.A., Voeltz G.K. (2008) – The reticulon and DP1/YOP1p proteins form immobile oligomers in the tubular endoplasmic reticulum. *J Biol Chem.* 283, 18892-904.

Shibata Y., Hu J., Kozlov M.M., Rapoport T.A. (2009) – Mechanisms shaping the membranes of cellular organelles. *Annu Rev Cell Dev Biol.* 25, 329-54.

Shibata Y., Shemesh T., Prinz W., Palazzo A., Kozlov M.M., Rapoport T.A. (2010) – Mechanisms determining the morphology of the peripheral ER. *Cell.* 143, 774-788.

Sparkes I., Tolley N., Aller I., Svozil J., Osterrieder A., Botchway S., Frigerio L., Hawes C. (2010) – Five plant reticulon isoforms share ER location, topology and membrane shaping properties. *Plant Cell.* 22, 1333-1343.

Stefano G., Hawes C., Brandizzi F. (2014) – ER – the key to the highway. *Curr Opin Plant Biol.* 22, 30-38.

Steiner P., Kulangara K., Sarria J.C., Glauser L., Regazzi R., Hirling H. (2004) – Reticulon 1-C/neuroendocrine-specific protein C interacts with SNARE proteins. *J Neurochem.* 89, 569-580.

Suetsugu S., Kurisu S., Takenawa T. (2014) – Dynamic of cellular membranes by phospholipids and membrane-deforming proteins. *Physiol Rev.* 94, 1219-1248.

Sundborger A.C. & Hinshaw J.E. (2014) – Regulating dynamin dynamics during endocytosis. *Prime Rep.* 6, 85.

Teng F.Y.U. & Tang B.L. (2008) – Cell autonomous function of Nogo and Reticulons: the emerging story at the endoplasmic reticulum. *J Cell Physiol.* 216, 303-308.

Terasaki M., Chen L.B., Fujiwara K. (1986) – Microtubules and the endoplasmic reticulum are highly interdependent structures. *J Cell Biol.* 103, 1557-1568.

Terasaki M. & Jaffe L.A. (1991) – Organization of the sea urchin egg endoplasmic reticulum and its reorganization at fertilization. *J Cell Biol.* 114, 929-940.

Terasaki M., Slater N.T., Fein A., Schmidek A., Reese T.S. (1994) – Continuous network of endoplasmic reticulum in cerebellar Purkinje neurons. *Proc Natl Acad Sci U S A.* 91, 7510-7514.

Terasaki M. (2000) – Dynamics of the endoplasmic reticulum and Golgi apparatus during early sea urchin development. *J Cell Biol.* 114, 929-940.

Tolley N., Sparkes I., Craddock C.P., Eastmond P.J., Runions J., Hawes C., Frigerio L. (2010) – Transmembrane domain length is responsible for the ability of a plant reticulon to shape endoplasmic reticulum tubules *in vivo*. *Plant J.* 64, 411-8.

Van de Velde H.J., Roebroek A.J., Senden N.H., Ramaekers F.C., Van de Ven W.J. (1994) – NSP-encoded reticulons, neuroendocrine proteins of a novel gene family associated with membranes of the endoplasmic reticulum. *J Cell Sci.* 107, 2403-2416.

Vedrenne C. & Hauri H.P. (2006) – Morphogenesis of the endoplasmic reticulum: beyond active membrane expansion. *Traffic.* 7, 639-646.

Voeltz G.K., Prinz W.A., Shibata Y., Rist J.M., Rapoport T.A. (2006) – A class of membrane proteins shaping the tubular endoplasmic reticulum. *Cell.* 124, 573-586.

Voeltz G.K. & Friedman J.R. (2011) – The ER in 3D: a multifunctional dynamic membrane network. *Trends Cell Biol.* 21, 709-17.

Wakefield S. & Tear G. (2006) – The *Drosophila* reticulon, Rtnl-1, has multiple differentially expressed isoforms that are associated with a sub-compartment of the endoplasmic reticulum. *Cell Mol Life Sci.* 63, 2027-38.

Waterman-Storer C.M. & Salmon E.D. (1998) – Endoplasmic reticulum membrane tubules are distributed by microtubules in living cells using three distinct mechanisms. *Curr Biol.* 8, 789-806.

Yang Y.S. & Strittmatter S.M. (2007) – The reticulons: a family of proteins with diverse functions. *Genome Biol.* 8, 234.

Youle R.J. & van der Bliek A.M. (2012) – Mitochondrial fission, fusion and stress. *Science.* 337, 1062.

Zhao X., Alvarado D., Rainier S., Lemons R., Hedera P., Weber C.H., Tukel T., Apak M., Heiman-Patterson T., Ming L., Bui M., Fink J.K. (2001) – Mutations in a newly identified GTPase gene cause autosomal dominant hereditary spastic paraplegia. *Nat Genet.* 29, 326-3.

Zimmerberg J. & Kozlov M.M. (2006) – How proteins produce cellular membrane curvature. *Nat Rev Mol Cell Biol.* 7, 9-19.

Zhu P.P., Patterson A., Lavoie B., Stadler J., Shoeb M., Patel R., Blackstone C. (2003) – Cellular localization, oligomerization, and membrane association of the hereditary spastic paraplegia 3a (SPG3A) protein atlastin. *J Biol Chem.* 278, 49063-71.

Zhu P.P., Soderblom C., Tao-Cheng J.H., Stadler J., Blackstone C. (2006) – SPG3A protein atlastin-1 is enriched in growth cones and promotes axon elongation during neuronal development. *Hum Mol Genet.* 15, 1343-53.

Zurek N., Sparks L., Voeltz G.K. (2011) – Reticulon short hairpin transmembrane domains are used to shape ER tubules. *Traffic.* 12, 28-41.

Acknowledgements

Thanks to Andrea Daga's laboratory. Thanks to Vadim A. Frolov's laboratory for liposome experiments. Thanks to Federico Caicci and Francesco Boldrin for EM experiments.